

Material characterisation of replicated calcium silicate element masonry

Jafari, Samira; Esposito, Rita

Publication date

2017

Document Version

Final published version

Citation (APA)

Jafari, S., & Esposito, R. (2017). *Material characterisation of replicated calcium silicate element masonry*. Delft University of Technology.

Important note

To cite this publication, please use the final published version (if applicable).
Please check the document version above.

Copyright

Other than for strictly personal use, it is not permitted to download, forward or distribute the text or part of it, without the consent of the author(s) and/or copyright holder(s), unless the work is under an open content license such as Creative Commons.

Takedown policy

Please contact us and provide details if you believe this document breaches copyrights.
We will remove access to the work immediately and investigate your claim.

<i>Project number</i>	C31B67
<i>File reference</i>	C31B67WP1-11
<i>Date</i>	August 08, 2017
<i>Corresponding author</i>	Samira Jafari (s.jafari@tudelft.nl)

TU Delft Large-Scale Testing Campaign 2016

MATERIAL TESTS FOR THE CHARACTERISATION OF REPLICATED CALCIUM SILICATE ELEMENT MASONRY

Authors: Samira Jafari, Rita Esposito

*Collaborators: Iren Frana, Jakub Pawlowicz, Marina Damiola, Andrea
Maioli, Edwin Meulman*

Cite as: Jafari, S., Esposito, R. *Material tests for the characterisation of replicated calcium silicate element masonry. Report No. C31B67WP1-11, August 08 2017. Delft University of Technology.*

This document is made available via the website 'Structural Response to Earthquakes' and the TU Delft repository. While citing, please verify if there are recent updates of this research in the form of scientific papers.

All rights reserved. No part of this publication may be reproduced, stored in a retrieval system of any nature, or transmitted, in any form or by any means, electronic, mechanical, photocopying, recording or otherwise, without the prior written permission of TU Delft.

TU Delft and those who have contributed to this publication did exercise the greatest care in putting together this publication. This report will be available as-is, and TU Delft makes no representations of warranties of any kind concerning this Report. This includes, without limitation, fitness for a particular purpose, non-infringement, absence of latent or other defects, accuracy, or the presence or absence of errors, whether or not discoverable. Except to the extent required by applicable law, in no event will TU Delft be liable for on any legal theory for any special, incidental consequential, punitive or exemplary damages arising out of the use of this report.

This research work was funded by NAM Structural upgrading stream.

Table of Contents

1	Introduction.....	3
2	Nomenclature	4
2.1	Symbols.....	4
2.2	Abbreviations.....	6
3	Construction of the samples	7
4	Flexural and compressive strength of mortar.....	8
4.1	Testing procedure.....	8
4.2	Experimental results.....	8
5	Flexural strength of masonry unit.....	10
5.1	Testing procedure.....	10
5.2	Experimental results.....	11
6	Compression properties of masonry unit.....	15
6.1	Testing procedure.....	15
6.2	Experimental results.....	17
7	Density of calcium silicate element masonry	20
8	Compression properties of masonry	21
8.1	Testing procedure.....	21
8.2	Experimental results.....	23
9	Flexural strength of masonry	30
9.1	Testing procedure.....	30
9.2	Experimental results.....	32
10	Bond strength of masonry.....	37
10.1	Testing procedure.....	37
10.2	Experimental results.....	37
11	Shear properties of masonry	41
11.1	Testing procedure.....	41
11.2	Experimental results.....	42
12	Comparison with values proposed by standards.....	46
12.1	Characteristic compressive strength of masonry.....	46
12.2	Elastic modulus of masonry.....	47
12.3	Stress-strain relationship for masonry in compression.....	47
12.4	Characteristic out-of-plane flexural strengths of masonry.....	48
12.5	Characteristic shear properties of masonry	49
12.6	Comparison with Table F.2 in NPR 9998:2017.....	49
13	Summary and properties overview.....	51
	References	54
	Appendix A.....	55

1 Introduction

In the Netherlands, the demand for accelerating the construction process has led to replacing traditional brick masonry with larger masonry units assembled with a thin mortar layer. Accordingly, different masonry unit sizes ranging from bricks to larger elements have been produced by calcium silicate industry. Since the mid-1980s, the popularity of using this element masonry has been raising in practice regarding the construction of unreinforced masonry (URM) building.

Despite the widespread application of calcium silicate element masonry, knowledge regarding the seismic response of this material is limited in the literature. Furthermore, in literature no comprehensive studies have been conducted on calcium silicate element masonry to characterise the entire range of material properties. Therefore, an extensive characterisation of the mechanical properties of masonry is of importance. These parameters serve as input for the assessment tools such as numerical and analytical models. As a result, an experimental study on calcium silicate element masonry was conducted, within the "NAM Structural Upgrading Project" developed at TU Delft in 2016.

The current research program fulfils the dual purpose of gathering benchmarks for verifying numerical models and providing insight into the behaviour of calcium silicate element masonry at material level. By using well-designed displacement-control testing set-ups, the compression, bending and shear properties of masonry specimens were measured, indicating strength, stiffness and post-peak behaviour of calcium silicate element masonry. A set of required input masonry properties pursued within this research is listed in Table 1. The testing procedure for each test has been defined in the related testing protocol [1].

A comprehensive overview of the behaviour of masonry constituents (element and mortar) and masonry at material level is reported in this document. The flexural and compressive strength of mortar and masonry unit (element) is provided from Section 4 to Section 6. The density of masonry is reported in Section 7. The compression, bending and shear properties of masonry are reported from Section 8 to Section 11. A comparison between experimental results and those values specified in the standards is reported in Section 12. Eventually, a summary and an overview of the material properties are reported in Section 13.

Table 1 – Destructive material tests for the characterisation of masonry.

		Type of test	Material property	
Mortar	Compression		Compressive strength of masonry mortar	
	Bending		Flexural strength of masonry mortar	
Masonry units	Compression		Compressive strength of unit Stress-strain relationship in compression Young's modulus of unit	
	Bending		Flexural strength of unit Elastic modulus of unit Stress-strain relationship in bending	
Masonry	Compression	Vertical	Compressive strength Young's modulus Fracture energy in compression	
		Horizontal	Poisson ratio Stress-strain relationship in compression (pre- and post-peak)	
	Bending	Out-of-plane	Vertical	Flexural strength with plane of failure parallel to bed joints Stress-strain relationship
			Horizontal	Flexural strength with plane of failure perpendicular to bed joints Stress-strain relationship
		In-plane	Vertical	Flexural strength with the moment vector perpendicular to the plane of the wall Stress-strain relationship
	Shear	Test on couplet		Initial shear strength Initial shear friction coefficient
Bond wrench			Flexural bond strength	

2 Nomenclature

2.1 Symbols

This report adopts mainly the nomenclature used in Eurocode 6 [2]. In addition, symbols used in the codes for testing are adopted.

α	Masonry (bed joint) angle of internal friction
ν	Poisson ratio of masonry
μ	Masonry (bed joint) coefficient of friction
μ_{ik}	Masonry (bed joint) characteristic coefficient of friction
ε_p	Strain associated with peak strength in vertical compression test
$\varepsilon_{p,h}$	Strain associated with peak strength in horizontal compression test
κ	Curvature of masonry subjected to bending load evaluated in the linear elastic phase
δ	Shape factor
d_1	Distance between bearing supports
d_2	Distance between loading supports
d_3	Distance between the loading and bearing supports (four-point bending test)
f_b	Normalised compressive strength of masonry unit
f_b^*	Compressive strength of masonry unit
f_{bt}	Flexural strength of masonry unit
f_{btIP}	Flexural strength of masonry unit subjected to in-plane bending
f_{ik}	Characteristic value of the i -th property
$f_{ik,EC6}$	Characteristic value of the i -th property as prescribed by Eurocode 6
$f_{ik,NPR}$	Characteristic value of the i -th property as prescribed by NPR 9096-1-1:2012
$f_{ik,NPR9998}$	Characteristic value of the i -th property as prescribed by NPR 9998:2017
f_m	Compressive strength of masonry mortar
f_{mt}	Flexural strength of masonry mortar
f_m'	Compressive strength of masonry in the direction perpendicular to the bed joints
$f_{m,h}'$	Compressive strength of masonry in the direction parallel to the bed joints
f_p	Applied lateral pre-compression stress
f_{x1}	Masonry flexural strength with the moment vector parallel to the bed joints and in the plane of the wall, which generates a plane of failure parallel to the bed joints
f_{x2}	Masonry flexural strength with the moment vector orthogonal to the bed joints and in the plane of the wall, which generates a plane of failure perpendicular to the bed joints
f_{x3}	Masonry flexural strength with the moment vector orthogonal to the plane of the wall
f_{v0}	Masonry (bed joint) initial shear strength for standard triplet
f_w	Masonry uniaxial bond strength between the masonry unit and the mortar
l_j	Length of the mortar bed joint in a masonry specimens

l_m	Length of the mortar specimen
l_s	Length of the masonry specimen as built
l_p	Length of the loading plate for compression tests on mortar specimens
l_u	Length of the masonry unit as used in the construction of masonry
h_m	Height of the mortar specimen
h_s	Height of the masonry specimen as built
h_u	Height of the masonry unit as used in the construction
t_s	Thickness of the masonry specimen as built
t_m	Thickness of the mortar specimen
t_u	Thickness of the masonry unit as used in the construction of masonry
v_{el}	Vertical displacement corresponding to the load F_{el}
A_s	Cross sectional area of the specimen parallel to the bed joints (shear test)
E_1	Secant elastic modulus of masonry subjected to a compressive loading perpendicular to the bed joints, evaluated at 1/3 of the maximum stress
E_2	Secant elastic modulus of masonry subjected to a compressive loading perpendicular to the bed joints, evaluated at 1/10 of the maximum stress
E_3	Chord elastic modulus of masonry subjected to a compressive loading perpendicular to the bed joints, evaluated at between 1/10 and 1/3 of the maximum stress
$E_{1,h}$	Secant elastic modulus of masonry subjected to a compressive loading parallel to the bed joints, evaluated at 1/3 of the maximum stress
$E_{2,h}$	Secant elastic modulus of masonry subjected to a compressive loading parallel to the bed joints, evaluated at 1/10 of the maximum stress
$E_{3,h}$	Chord elastic modulus of masonry subjected to a compressive loading parallel to the bed joints, evaluated at between 1/10 and 1/3 of the maximum stress
E_b	Elastic modulus of masonry unit obtained from compression test
E_{bt}	Elastic modulus of masonry unit obtained from three-point (out-of-plane) bending test
E_{btIP}	Elastic modulus of masonry unit obtained from three-point in-plane bending test
E_{fx1}	Elastic modulus of masonry in bending parallel to the bed joints
E_{fx2}	Elastic modulus of masonry in bending perpendicular to the bed joints
F_1	Applied vertical load (bond-wrench test)
F_2	Vertical load due to the weight of the top clamping system (bond-wrench test)
F_3	Vertical load due to the top masonry unit (bond-wrench test)
F_{max}	Maximum vertical load
$F_{joint-crack}$	Peak load corresponding to the development of the vertical crack in the joint
F_{el}	Selected vertical load value in the linear elastic stage (flexural test of masonry unit)
F_p	Applied lateral pre-compression force (shear test)
G_{f-c}	Fracture energy in compression for loading perpendicular to the bed joints
$G_{f-c,h}$	Fracture energy in compression for loading parallel to the bed joints
G_{fx1}	Fracture energy in tension parallel to the bed joints
G_{fx2}	Fracture energy in tension perpendicular to the bed joints

G_{fib}	Fracture energy in bending for masonry unit
M_{max}	Maximum bending moment
W	Section modulus
I	Moment of inertia of the masonry unit along the cross-section

2.2 Abbreviations

Avg.	Average
C.o.V.	Coefficient of variation
CS	Calcium silicate
LVDT	Linear variable differential transformer
St. dev.	Standard deviation

3 Construction of the samples

The masonry specimens were built in the Stevin II laboratory at Delft University of Technology. The masonry was made of calcium silicate element assembled together with very thin layer of mortar. A premixed mortar was used stored in bags of 25 kg. During the preparation of the mortar 6 litre of water per bag was used. On average one batch of mortar per construction day was use. The calcium silicate elements are roughly 897x643x100-mm (Figure 1a). Each element is made with a tongue and groove connection on the side to facilitate the construction process. Due to the weight of each single element (approximately 100 kg), a crane was used to assemble the construction (Figure 1b). Two holes on the top side of each element are present to provide support for crane hooker (Figure 2a), while during the construction they were filled by plastic tools designed for this purpose (Figure 2b). The declarations of performance of the materials are reported in Appendix A.

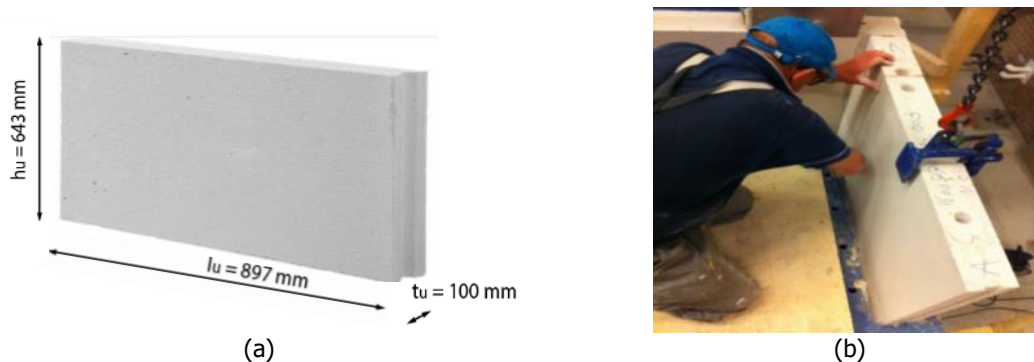


Figure 1 – Calcium silicate element: (a) with dimensions of 897x643x100-mm; (b) small crane to lift the element.

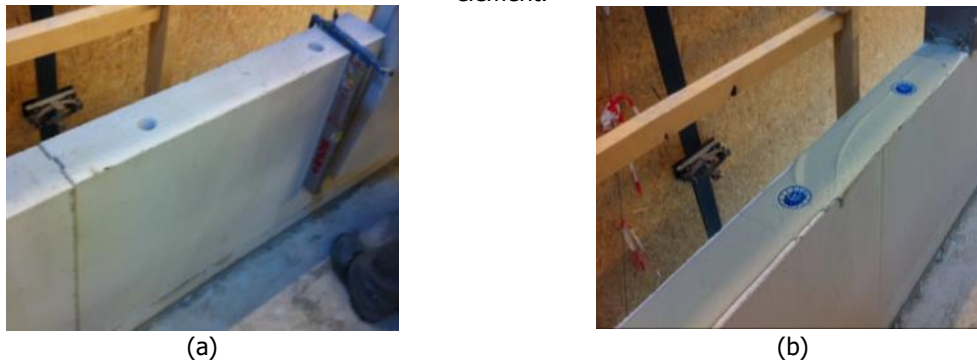


Figure 2 – Calcium silicate element: (a) holes are present on the top side; (b) plastic tools used to fill the holes.

In order to ensure quality control, the construction followed the prescription as reported in the construction protocol [3]:

- The bags of mortar mix were stored dry and separated from the soil;
- The mortar mix was used within 18 months after production;
- The mortar was mixed with clean water;
- The mortar was prepared using a fixed water content;
- The flow of the mortar was determined in agreement with EN 1015-3:1999 [4].
- At least three samples of mortar (size 160x40x40 mm³) were made at every start of the day during construction of masonry for testing the properties. The samples were tested under flexural and compressive loading in agreement with EN 1015-11:1999 [5];
- The mortar was prepared and used between 5 and 25 degrees;
- No additives were mixed after preparation of the mortar;
- Elements were covered against moisture;
- Elements were clean before use;

The mortar was prepared with fixed water content per bag of mix (25 kg): 6.0 l/bag for calcium silicate element masonry.

4 Flexural and compressive strength of mortar

During the masonry construction, mortar samples were collected and cast in moulds to be tested for the flexural and compressive strength in agreement with EN 1015-11:1999 [5]. The consistency of the mortar was determined in accordance with EN 1015-3:1999 [4].

4.1 Testing procedure

Mortar bar specimens having a length of $l_m = 160$ mm, a height of $h_m = 40$ mm and thickness of $t_m = 40$ mm. During each day of construction at least three mortar bars were collected. The samples were stored in controlled conditions. The first two days they were placed in a fog room ($T = 20 \pm 2^\circ\text{C}$, $\text{RH} = 95 \pm 5\%$) with the moulds. After two days, they were un moulded and kept for other five days in the fog room. Eventually, they were placed in a conditioning room with a temperature of $20 \pm 2^\circ\text{C}$ and a relative humidity of $50 \pm 5\%$ until testing. The test was performed after at least 28 days from construction.

The flexural strength was determined by three-point bending test (Figure 3a). The test set-up is composed by two steel bearing rollers having a diameter of 10 ± 0.5 mm and spaced $d_l = 100 \pm 0.5$ mm. A third roller is centrally placed on top of the sample to apply the load.

The compression test was performed on the broken pieces obtained from the flexural test, which have at least a length of 40 mm. The specimen is placed between two steel plates with a length of $l_p = 40$ mm. For the interpretation of the results the specimens considered to be 40x40x40-mm (Figure 3b).

For both tests, the load was applied without shock at a uniform rate so that failure occurred within a period of 30 to 90 s. The maximum load was recorded.



Figure 3 – Test on masonry mortar specimens: (a) three-point bending test; (b) compression test.

4.2 Experimental results

The flexural strength f_{mt} of the mortar was calculated as [5]:

$$f_{mt} = \frac{3 F_{\max} d_l}{2 t_m h_m^2} \quad (1)$$

where F_{\max} is the maximum load, d_l is the distance between the supports ($100 \text{ mm} \pm 0.5 \text{ mm}$), h_m is the height of the mortar specimen (40 mm) and t_m is the thickness of the mortar specimen (40 mm).

The compressive strength f_m of the mortar was calculated as [5]:

$$f_m = \frac{F_{\max}}{t_m l_p} \quad (2)$$

where F_{max} is the maximum load, t_m is the thickness of the mortar specimen (40 mm) and l_p is the length of the loading plate (40 mm).

During the masonry construction, the slump test was performed after the preparation of mortar in the beginning of the day. The diameter of the cone was obtained in agreement with the slump test described in EN 1015-3:1999 [4]. The measured diameter varied between 178 to 190 mm (see Table 2).

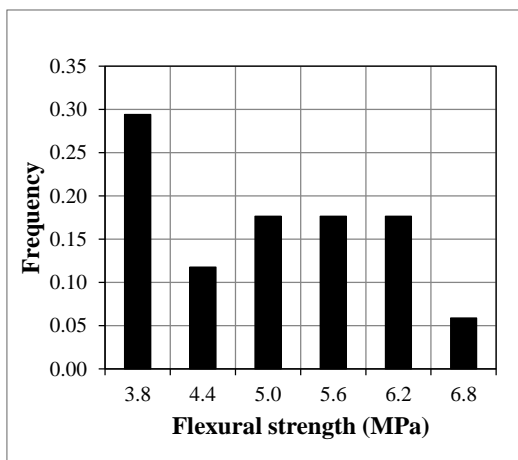
Table 2 – Consistency of calcium silicate element masonry mortar measured during construction.

Casting date	Cast number	Flow (mm)
19-10-2016	1	190
20-10-2016	1	185
26-10-2016	1	189
27-10-2016	1	185
02-11-2016	1	185
03-11-2016	1	178
Average		185

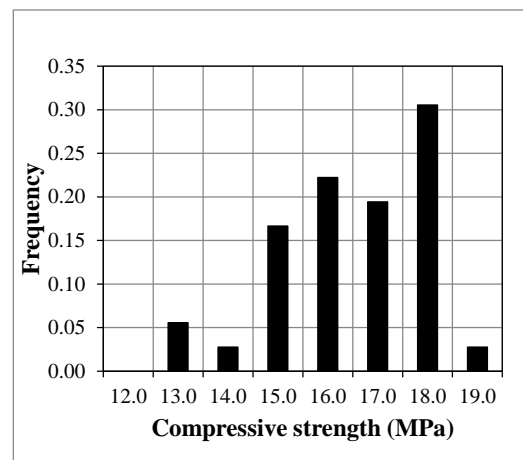
The flexural and compression tests on the hardened mortar were performed at least after 28 days. Table 3 lists the results for the three-point bending tests and compression tests. These results for each day were calculated considering the average results of the three mortar bars. Three-point bending tests were performed on 18 specimens and compressive tests were conducted on 36 specimens. The mortar has a compressive strength of 16.1 MPa and flexural strength of 4.7 MPa. The mean values of the properties are calculated as the average of all the test results. Statistical distribution of mortar strength is shown in Figure 4.

Table 3 – Flexural and compressive strength of calcium silicate element masonry mortar.

Casting date	Companion sample	Flexural tests			Compression test		
		f_{mt} (MPa)	St. dev.	C.o.V.	f_m (MPa)	St. dev.	C.o.V.
19-10-2016	COMP25/28/29	5.9	0.20	0.03	17.5	0.43	0.02
20-10-2016	COMP24-MAT51-g/h/i/j	3.6	0.07	0.02	13.9	0.84	0.06
26-10-2016	MAT52/53	4.2	0.28	0.07	16.6	1.20	0.07
27-10-2016	MAT53/54	3.9	0.87	0.22	16.4	0.65	0.04
02-11-2016	MAT-51-a/b/c/d	5.6	0.82	0.15	16.8	0.89	0.05
03-11-2016	MAT-51-e/f+ MAT55/56	4.6	0.78	0.17	15.5	1.41	0.09
Average all casts		4.7	1.04	0.22	16.1	1.48	0.09
Standard deviation							
Coefficient of variation							



(a)



(b)

Figure 4 – Statistical distribution of mortar strength: (a) flexural strength; (b) compressive strength.

5 Flexural strength of masonry unit

The flexure strength of the masonry unit was determined with the three-point bending test following NEN 6790:2005 [6]. The test was also used to determine the elastic modulus of the masonry unit.

5.1 Testing procedure

To investigate the flexural strength of CS element, two types of samples were adopted as follows:

- Sawn-cut specimens having dimensions 200x100x100-mm. Following NEN 6790:2005 [6], the (out-of-plane) flexural strength of one large masonry unit could be represented by performing tests on three small pieces sawn-cut from bottom, middle and top side of one single element. Tests were performed on 18 specimens extracted out of 6 full-scale elements, see Figure 5.
- Full-scale elements having dimensions 897x643x100-mm. In-plane bending test was conducted to investigate the softening behaviour of the element. Totally, four samples were tested.

The sawn-cut specimens were tested by having the bed joint plane parallel to the loading direction (Figure 6b). The specimen was supported by two roller bearings, which were placed 10 mm from the end of the specimen. A third roller was used to apply load to the specimen at mid-span. The test was carried out by a displacement controlled apparatus including a hydraulic jack with 50 kN capacity. A spherical joint, between the upper roller and hydraulic jack, was used to minimise load eccentricity. To obtain the failure of the specimen in 30 to 90 s, a displacement rate of 0.02 mm/s was adopted. The applied load was recorded from the load cell attached to the hydraulic jack. Two LVDTs were attached to the specimens to measure horizontal and vertical displacements. On the front side, a horizontal LVDT measured the elongation between two points on the masonry unit. On the back side the vertical displacement at mid-span of the masonry unit, relative to its supports, was measured. The LVDTs had a measuring range of 10 mm with an accuracy of 0.1%.

The full-scale element was tested by having the bed joint perpendicular to the loading direction (Figure 6b). The specimen was supported by two roller bearings, which were placed 45 mm from the end of the specimen. A third roller was used to apply load to the specimen at mid-span. The test was carried out by a displacement controlled apparatus including a hydraulic jack with 100 kN capacity. A spherical joint, between the upper roller and hydraulic jack, was used to minimise load eccentricity. A displacement rate of 0.002 mm/s was adopted. The applied load was recorded from the load cell attached to the hydraulic jack. To direct a crack that initiates in the middle of the unit, a notch was made with depth of 2 ± 1 cm.

Twelve LVDTs were attached to the specimens to measure horizontal and vertical displacements. On both sides, a horizontal LVDT measured the crack opening on the masonry unit. To gain insight into the softening post-peak behaviour, the crack opening was used as a parameter to control displacement of the jack. The horizontal LVDTs had a measuring range of 2 mm with an accuracy of 0.1%.

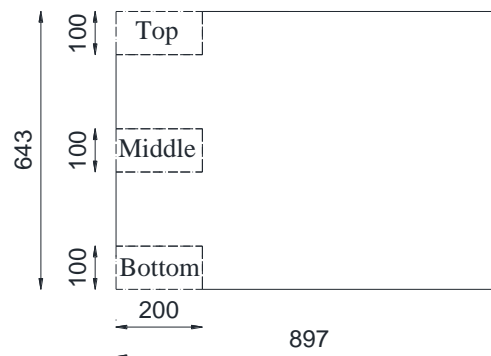


Figure 5 – Bending test on CS element sawn-cut from full-scale element (TUD-E54), dimensions are in mm.

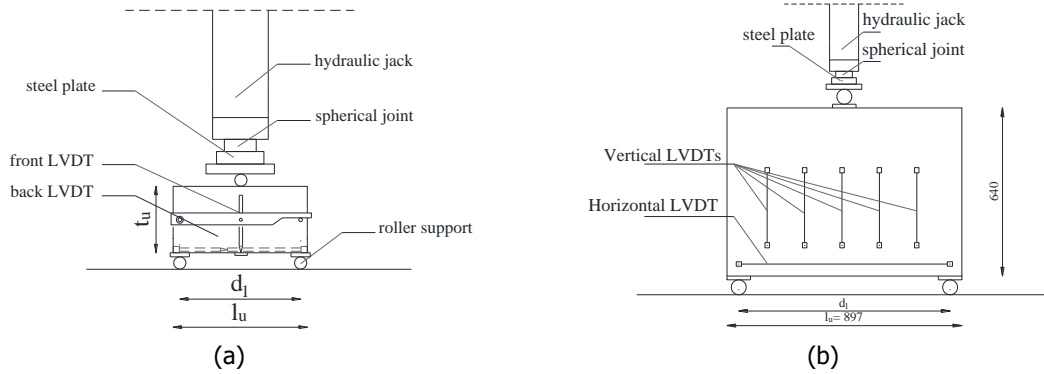


Figure 6 – Three point bending tests: (a) sawn-cut specimens (TUD-E-54); (b) in-plane bending test on full-scale element (TUD-E-55).

5.2 Experimental results

For the sawn-cut specimens tested in three-point out-of-plane bending, the flexural strength of the masonry unit f_{bt} was determined as [6]:

$$f_{bt} = \frac{3 F_{max} d_1}{2 h_u t_u^2} \quad (3)$$

where F_{max} is the maximum load, d_1 is the distance between the supports, h_u is the height of the sawn-cut masonry specimen, t_u is the thickness of the masonry unit.

Assuming a linear stress distribution over the height of the cross-section, the elastic modulus E_{bt} of the masonry units can be determined as follows:

$$E_{bt} = \frac{F_{el} d_1^3}{48 v_{el} I} \quad (4)$$

where F_{el} and v_{el} are the load and vertical displacement in the linear elastic stage, respectively and I is the moment of inertia of the masonry unit along the cross-section.

For the full-scale specimens tested in three-point in-plane bending, the flexural strength of the masonry unit f_{btIP} was determined as:

$$f_{btIP} = \frac{3 F_{max} d_1}{2 t_u h_u^2} \quad (5)$$

where F_{max} is the maximum load, d_1 is the distance between the supports, h_u is the height of the full-scale masonry unit, t_u is the thickness of the masonry unit.

The elastic modulus is determined from the horizontal LVDTs as follows:

$$E_{btIP} = \frac{M}{I \kappa} \quad (6)$$

where M is the bending moment in the linear elastic stage, I is the moment of inertia of the masonry unit along the cross-section and κ is the curvature determined as strain calculated from the horizontal LVDTs readings in the linear elastic stage divided by the vertical distance of the LVDTs from the neutral axis.

Figure 7 shows the flexural stress versus horizontal and mid-span displacement for the sawn-cut specimens. As can be seen in Figure 7, for all the sawn-cut specimens a brittle failure was reported. A typical crack pattern observed during the tests is shown in Figure 8. The results of flexural strength and elastic modulus are listed in Table 4 and reported in Figure 11a with histogram representation.

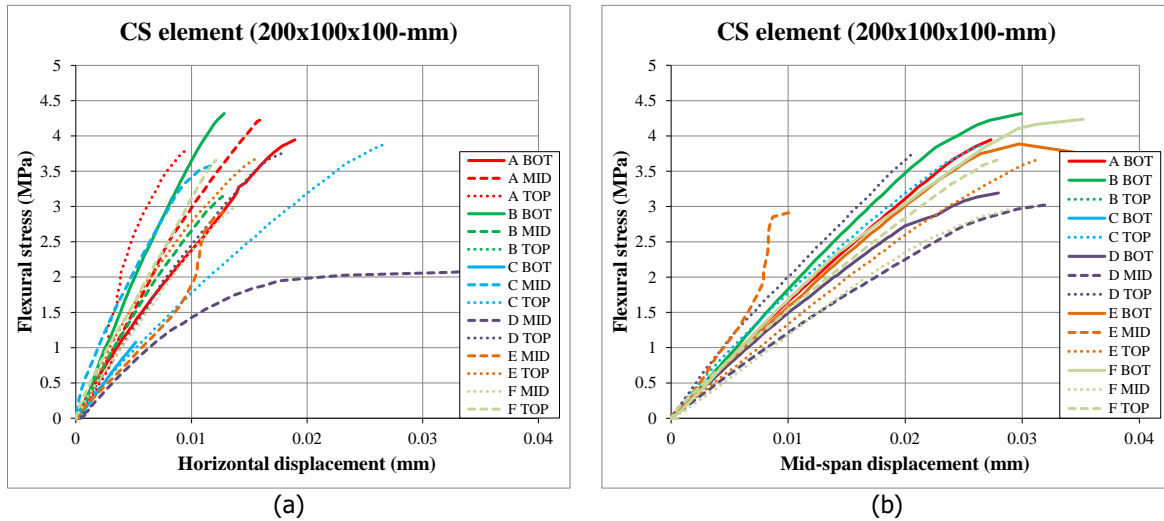


Figure 7 – Flexural stress-displacements curve (LVDTs readings) of three-point bending test on sawn-cut specimens of calcium silicate element: (a) horizontal displacements; (b) vertical displacements in the middle of the brick.



Figure 8 – Crack pattern for sawn-cut specimens (200x100x100-mm): (a) symmetric crack pattern; (b) asymmetric crack pattern.

Table 4 – Bending properties for the sawn-cut specimens (200x100x100-mm).

Sawn-cut specimens (200x100x100-mm)							
Sample name		f_{bt}		E_{bt}		G_{fbt}	
		MPa		MPa		N/mm	
TUD_E-54A	bottom	3.95		9385		0.021	
	middle	4.24	4.0	-	9385	-	0.021
	top	3.82		-		-	
TUD_E-54B	bottom	4.32		10165		0.027	
	middle	3.14	3.73	-	7617	-	0.027
	top*	1.86		5070		-	
TUD_E-54C	bottom*	3.24		-		-	
	middle	3.57	3.73	-	9852	-	-
	top	3.89		9852		-	
TUD_E-54D	bottom	3.19		8181		0.020	
	middle	3.02	3.32	6622	8851	0.021	0.019
	top	3.75		11750		0.016	
TUD_E-54E	bottom	3.89		8618		0.024	
	middle	2.92	3.49	12144	9324	-	0.024
	top	3.67		7209		0.023	
TUD_E-54F	bottom	4.24		8633		0.034	
	middle	2.97	3.62	6027	7658	0.018	0.025
	top	3.66		8314		0.021	
Average		3.64	3.65	8613	9206	0.023	0.023
Standard deviation		0.45	0.21	2006	807	0.005	0.003
Coefficient of variation		0.12	0.06	0.23	0.09	0.22	0.13

* Results are excluded from the average due to formation of asymmetric crack

Figure 9 shows the moment-curvature curve for the full-scale elements. The crack opening, measured as average values of horizontal LVDTs, was used as a parameter to control the jack displacement. Consequently, the post-peak behaviour was investigated. A typical crack pattern observed during the tests is shown in Figure 10. The results of flexural strength and elastic modulus are listed in Table 5 and reported in Figure 11b with histogram representation.

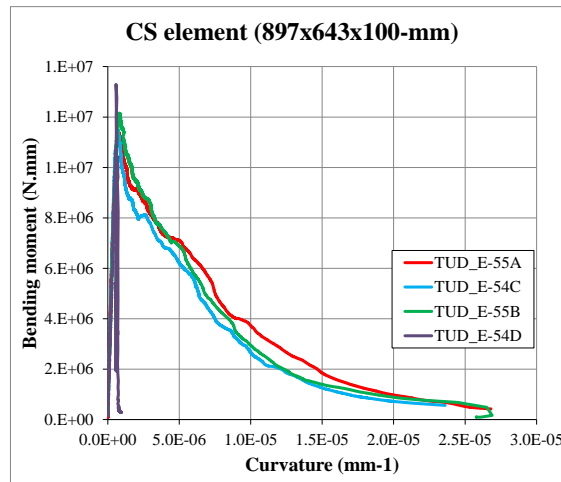


Figure 9 – Moment-curvature curve for full-scale calcium silicate element subjected to in-plane bending test.

Table 5 - Bending properties for the full-scale calcium silicate element (897x643x100-mm) subjected to in-plane bending.

Full-scale CS element (897x643x100-mm)		
Sample name	f_{btIP}	E_{btIP}
	MPa	MPa
TUD_E-55A	1.78	11569
TUD_E-55B	1.84	8643
TUD_E-55C	1.74	10359
TUD_E-55D	1.76	5973
Average	1.78	8325
Standard deviation	0.04	1805
Coefficient of variation	0.02	0.22



Figure 10 – Symmetric crack pattern for full-scale calcium silicate element subjected to three point in-plane bending (897x643x100-mm).

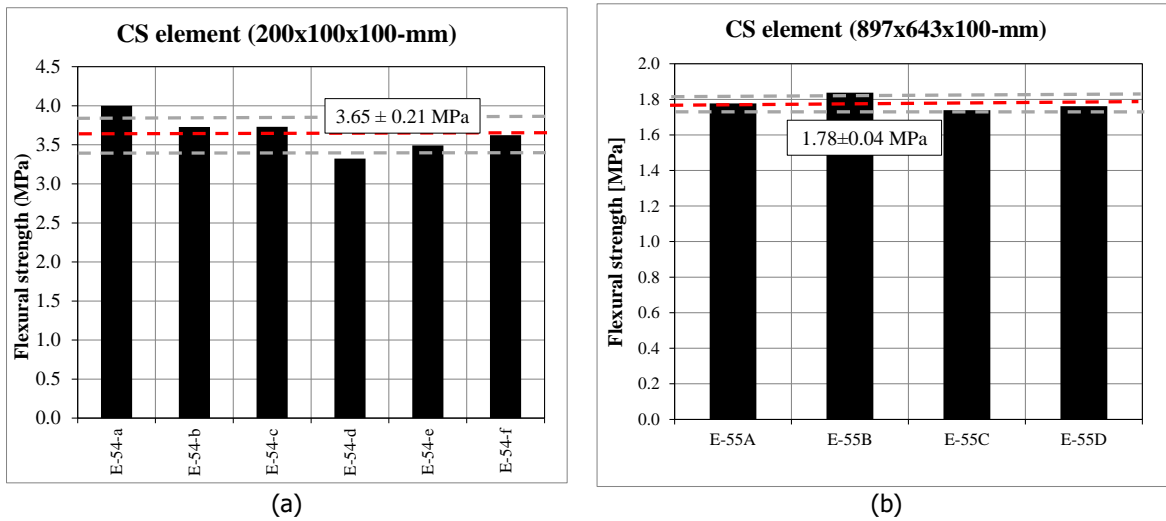


Figure 11 – Flexural strength values of calcium silicate element: histogram representation; (a) sawn-cut specimens (200x100x100-mm); (b) full-scale element (897x643x100-mm) subjected to in-plane bending.

6 Compression properties of masonry unit

The compressive strength and the Young's modulus of CS element are determined by performing compression tests. The test is performed following EN 772-1:2000 [7]. Additional test configuration was adopted to investigate the possible size effect on the compression properties.

6.1 Testing procedure

To investigate the compression properties of CS element, three types of samples were adopted as follows:

- Sawn-cut specimens having dimensions 100x100x100-mm (TUD-E-51). Following EN 771-2 [8], the compression strength of one large masonry unit could be represented by performing tests on three small sawn-cut specimens extracted from the bottom, the middle and the top side of one single element. Tests were performed on 18 specimens extracted out of 6 full-scale elements.
- Sawn-cut specimens having dimensions 225x450x100-mm (TUD-E-52), thus a height-to-thickness ratio (h_u/t_u) equal to 4.5, as suggested by Vermeltfoort [9]. The specimens were used to evaluate the Young's modulus. Tests were performed on 6 specimens extracted out of 6 full-scale elements. The specimens were extracted from the same elements used for the extraction of the 100x100x100-mm specimens, see Figure 12.
- One full-scale element having dimensions 897x643x100-mm (TUD-E-53) was tested.

Tests on the sawn-cut specimens, both TUD-E-51 and TUD-E-52, were carried out through a displacement-controlled apparatus including a hydraulic jack with 300-ton capacity. The hydraulic jack lifts a steel plate, the active side, and there is a passive load plate at the top. A hinge between the load cell and the top steel plate reduces possible eccentricities during loading. A load cell that measures the applied force is attached to the top steel plate.

Since the small height of the samples with 100x100x100-mm dimensions was not allowed attaching LVDTs in this dimension, four vertically oriented LVDTs were attached to the machine platens in order to measure relative vertical displacements (see Figure 13a). Their measuring range is 10 mm with an accuracy of 0.1%. The rate of the jack displacement was set to 0.01 mm/s so that failure was reached not less than approximately 60 seconds, according to the standard [7].

The TUD-E-52 samples, which were adopted with the aim to evaluate the Young's modulus, were instrumented with 3 LVDTs (2 longer ones on the sides and 1 smaller on the centre) both on the front and the back sides. In addition, two LVDTs were positioned between the centres of the loading plates (see Figure 13b). The rate of the jack displacement was set to 0.003 mm/s.

Test on the full-scale calcium silicate elements (TUD-E-53) was conducted using the testing apparatus provided with a hydraulic jack with approximately 200-ton capacity. A displacement-control set-up was designed for this purpose. The testing set-up was also used to compress the masonry wallets. The load imposed on the tested specimen was applied through two spreading beams, which are connected to the load cell by a hinge to reduce possible eccentricities during loading. The active side of the load system is in the top of the hydraulic jack. A load cell that measures the applied force is attached to the top steel plate. More information regarding the test set-up can be found in Section 7.

The TUD-E-53 sample was adopted aiming to evaluate the Young's modulus and compressive strength of full-scale element. The sample was instrumented with 3 LVDTs (2 longer ones on the sides and 1 smaller on the centre) both on the front and the back sides. In addition, four LVDTs were positioned between the loading plates (see Figure 13b). The rate of the jack displacement was set to 0.003 mm/s.

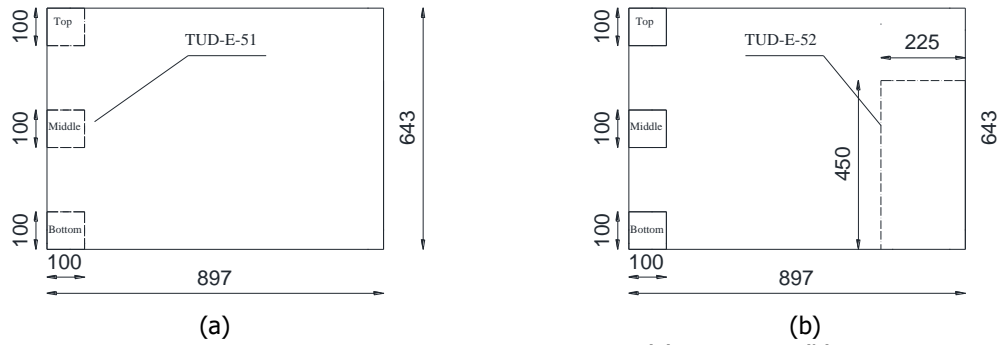


Figure 12 - Compression test on sawn-cut specimens: (a) TUD-E-51; (b) TUD-E-52.

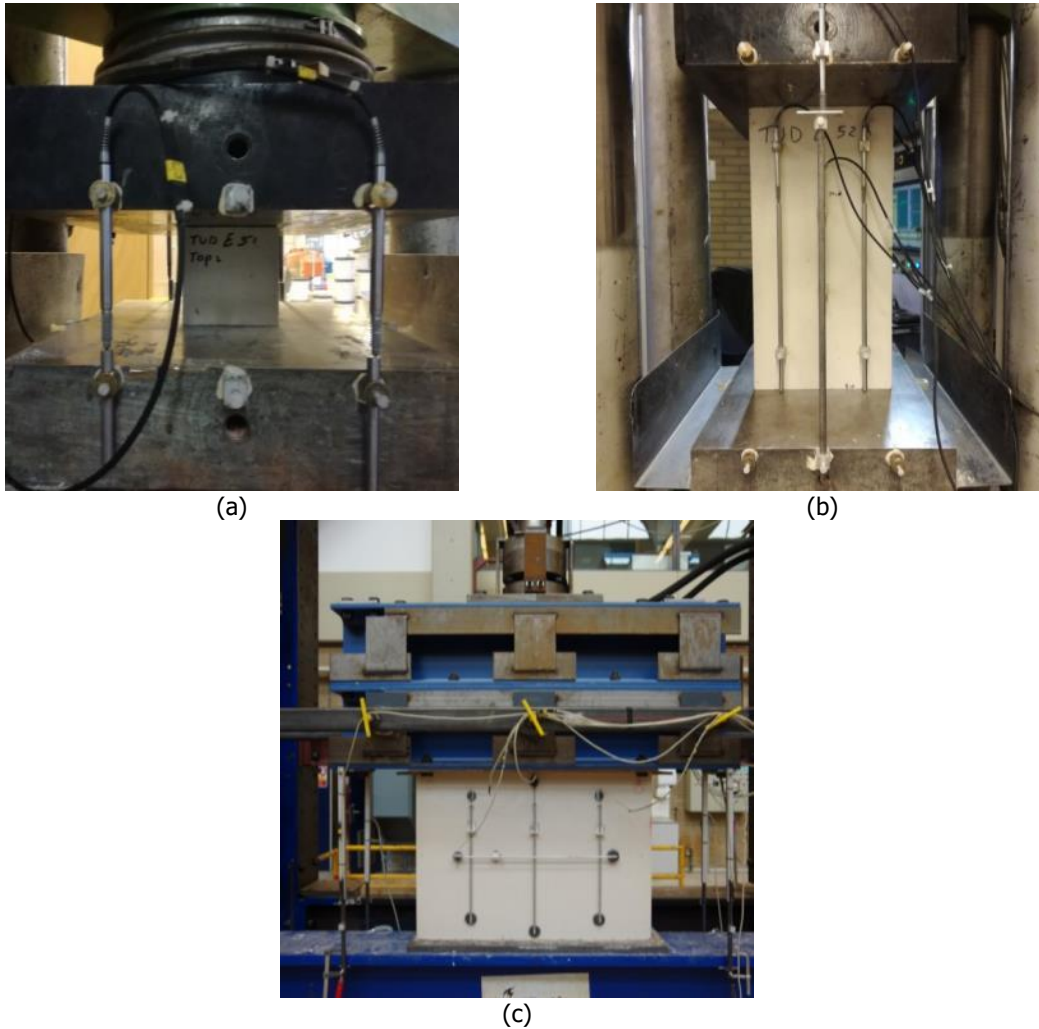


Figure 13 - Compression test on CS element units: (a) sawn-cut specimens (TUD-E-51) to find out the compressive strength; (b) sawn-cut specimens (TUD-E-52) to find out the Young's modulus; (c) compression test on full-scale element (TUD-E-53).

6.2 Experimental results

The compressive strength of the masonry unit f_b^* can be determined from test on single masonry unit as:

$$f_b^* = \frac{F_{\max}}{l_u \cdot t_u} \quad (7)$$

where F_{\max} is the maximum load, l_u and t_u are the length and thickness of the specimen respectively. Following the Annex A of standard EN 772-1 [7], the normalised compressive strength of the masonry unit f_b is determined as:

$$f_b = \delta \cdot f_b^* \quad (8)$$

where δ is the shape factor determined in agreement with Table A.1 in Ref. [7]. The shape factor used to normalise the compressive strength for the three types of the samples is as follows:

- $\delta=1.0$ for the sawn-cut specimens with 100x100x100-mm
- $\delta=1.2$ for the sawn-cut specimens with 250x450x100-mm
- $\delta=1.45$ for the full-scale element with 897x643x100-mm

The compressive strength, normalised compressive strength and the Young's modulus for the sawn-cut specimens are listed in Table 6. Figure 15 shows the results with the histogram representation. Considering the readings of the LVDTs' attached on the samples, the chord modulus was calculated between 1/10 and 1/3 of the maximum stress. As already mentioned no reliable values of Young's modulus can be obtained for the specimens TUD_E-51 due to the use of LVDT's between loading plates.

As already mentioned one full-scale element was subjected to compressive load. The compressive strength and the normalised compressive strength for the full-scale element were respectively 14.2 MPa and 20.6 MPa. The chord elastic modulus was equal to 7630 MPa.

Table 6 – Compression properties of the calcium silicate element.

Sawn-cut specimens (100x100x100-mm)					Sawn-cut specimens (250x450x100-mm)			
Sample name		f_b^*	f_b		Sample name	f_b^*	f_b	E_b
		MPa	MPa			MPa	MPa	MPa
E51-A	top	20.6	20.6	20.7	E52-A	18.1	21.7	9936
	mid	17.1	17.1					
	bot	24.2	24.2					
E51-B	top	21.6	21.6	20.4	E51-B	16.9	20.2	9677
	mid	14.0	14.0					
	bot	25.5	25.5					
E51-C	top	18.8	18.8	18.4	E52-C	14.5	17.4	8216
	mid	15.5	15.5					
	bot	21.1	21.1					
E51-D	top	18.8	18.8	18.5	E52-D	15.0	18.0	7894
	mid	15.7	15.7					
	bot	21.0	21.0					
E51-E	top	18.5	18.5	18.1	E52-E	15.9	19.0	8090
	mid	17.0	17.0					
	bot	18.7	18.7					
E51-F	top	21.8	21.8	20.7	E52-F	15.4	18.5	7803
	mid	17.3	17.3					
	bot	23.0	23.0					
Average		19.5	19.5	19.5	Average	16.0	19.2	8603
St. dev.		3.1	3.1	1.1	St. dev.	1.3	1.6	947
C.O.V		0.16	0.16	0.06	C.O.V	0.08	0.08	0.11

The observed type of the cracks for the three types of the tested samples can be summarised as follows:

- The sawn-cut specimens having dimensions 100x100x100-mm (TUD-E-51) showed vertical cracks parallel to the loading direction initiated from the sides of the specimen, see Figure 14a.
- The sawn-cut specimens having dimensions 250x450x100-mm (TUD-E-52) showed vertical and diagonal cracks with consequent spalling of part of the element, see Figure 14b.
- The full-scale specimen showed vertical crack parallel the loading direction, see Figure 14c. At peak stress, a horizontal crack at mid-height of the specimen formed leading to brittle failure, see Figure 14d.

Comparing the compression properties obtained from performing tests on the specimens with different dimensions, the following conclusions can be drawn:

- By increasing the dimensions of the specimens, lower values of the compressive strength f_b was found. However, a good agreement in terms of normalised compressive strength f_b was found for the specimens having different dimensions.
- Similar results in terms of chord elastic modulus E_b were obtained for the sawn-cut specimens (8603 MPa) and for the full-scale specimen (7630 MPa).

It can be concluded that by performing test on the sawn-cut specimens having dimensions 250x450x100-mm, a proper characterisation of the compression properties of masonry unit can be obtained.

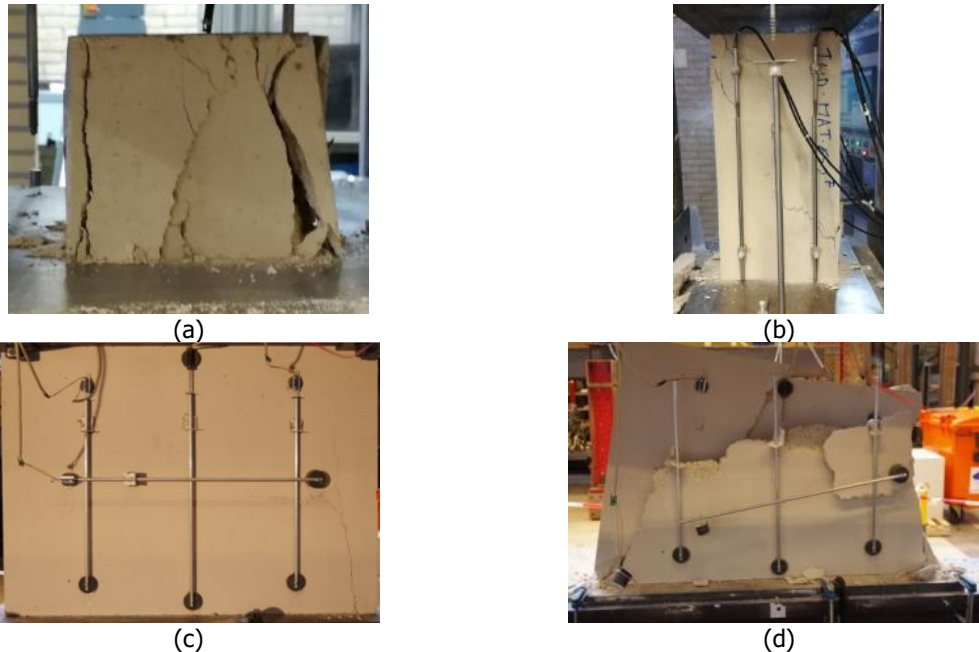
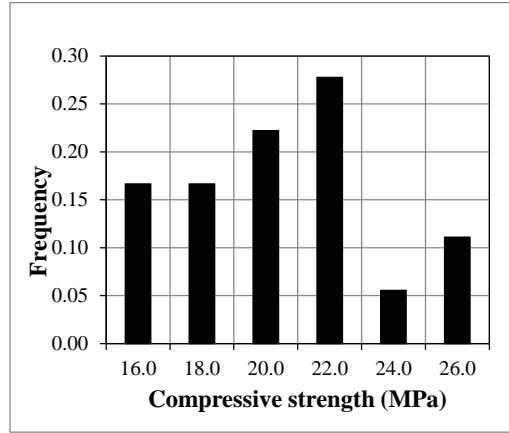
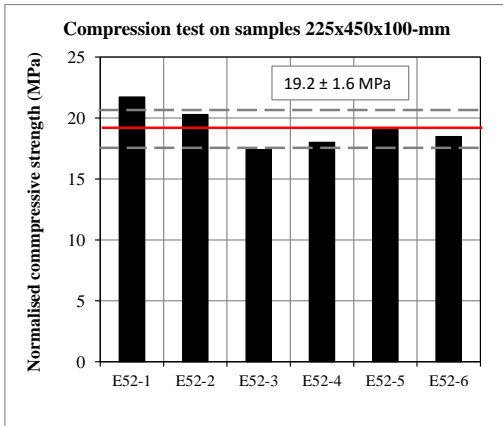


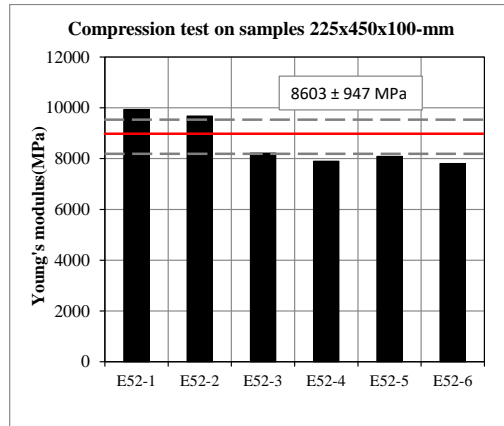
Figure 14 - Crack pattern for specimens subject to compression tests: sawn-cut specimens TUD-E-51; (b) sawn-cut specimens TUD-E-52; (c)-(d) full-scale element TUD-E-53.



(a)



(b)



(c)

Figure 15 – Statistical distribution of element compression properties: (a) compressive strength from tests on 18 sawn-cut specimens with 100x100x100-mm; (b) compressive strength and (c) Young's modulus from tests on 6 sawn-cut specimens with 225x450x100-mm.

7 Density of calcium silicate element masonry

To measure the density of the calcium silicate element masonry, weight and dimensions of the specimens adopted for the bond wrench test were measured prior to testing. The average value of the density for the calcium silicate element masonry is reported as 1824 kg/m³ as listed in Table 7.

Table 7 – Density of calcium silicate element masonry.

<i>L_s</i>	<i>h_s</i>	<i>t_s</i>	Weight	Density
mm	mm	mm	kg	Kg/m ³
221	126	99	4.93	1787
222	122	100	4.75	1754
222	125	100	4.87	1753
221	125	99	4.94	1804
217	120	99	4.72	1829
222	125	99	4.94	1796
218	118	99	4.59	1802
220	120	98	4.83	1865
216	123	99	4.75	1804
216	125	98	5.03	1901
215	122	99	4.80	1848
221	120	100	4.82	1816
221	123	98	4.93	1849
221	123	99	4.82	1791
217	124	99	4.93	1851
219	122	99	4.80	1815
218	126	100	5.06	1840
222	123	100	5.12	1873
217	120	100	4.83	1855
221	124	99	4.92	1812
221	121	98	4.89	1864
221	125	100	5.05	1828
Average				1824
Standard deviation				38
Coefficient of variation				0.02

8 Compression properties of masonry

The compression strength and elastic modulus of the masonry were determined in agreement with EN 1052-1:1998 [10]. Additional test configurations were adopted to investigate the orthotropic behaviour of the masonry and the cyclic response of the material.

8.1 Testing procedure

The size of the specimens was determined on the basis of the dimensions of the CS element unit in agreement with EN 1052-1:1998 [10]. The calcium silicate element masonry specimens have dimensions of 1283x1290x100-mm. The dimensions of the specimens were chosen following the standard, as shown in Figure 16. More information regarding the dimensions of the specimens can be found on Ref. [1]. A 10 mm thick layer of gypsum was applied to faces in contact with the loading plates, to ensure that the loaded faces of the specimens are levelled and parallel to one another. This was done to prevent additional stresses in the specimens.

The compression strength and elastic modulus of the masonry were determined in two orthogonal directions with respect to the bed joints. Two configurations were used: a *vertical configuration* in which the loading was perpendicular to the bed joints and a *horizontal configuration* in which the loading was parallel to the bed joint. The former is prescribed by the standard EN 1052-1:1998, while the latter is additionally used to investigate the orthotropic behaviour of the material.

A displacement-control set-up was designed to compress the large calcium silicate element masonry specimens. The set-up is composed of two identical steel frames positioned parallel to each other, connected on top and bottom. Each of the contrast frames is composed of two HEB300 columns and two HEB1000 beams. Bottom steel beam acts as a support for the tested specimen, while the top one holds the load cell. The testing apparatus was provided with a hydraulic jack of approximately 200-ton capacity. The load applied through two spreading beams, which are connected to the load cell by a hinge to reduce possible eccentricities during loading (Figure 17b). The system is operated in deformation control, using the displacement of the jack as control variable. A load cell that measures the applied force is attached to the top steel plate.

Four LVDTs (two on the sides) were attached to the specimen to register vertical relative displacements over the height of the specimen (Figure 18). They were installed as closely as possible to the surface of the specimen to reduce possible errors caused by rotation of the contact points to which they were attached. Their measuring range is 10 mm with an accuracy of 0.1%. Additionally, two LVDTs (one for each side) were attached to the specimen to register the horizontal relative displacement over the length of the specimen. Moreover, four LVDTs were positioned between the loading plates. Their measuring range is 25 mm with an accuracy of 0.1%.

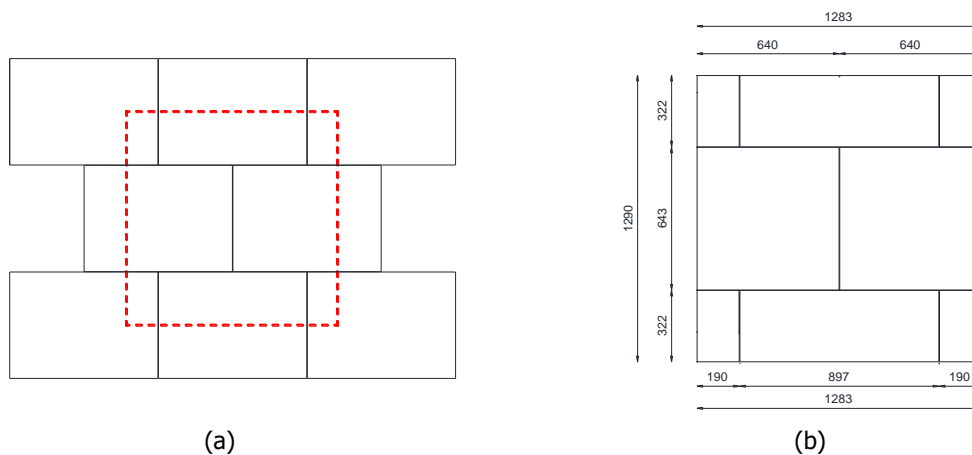


Figure 16 – Compression test on CS element masonry specimen: (a) tested portion; (b) dimensions of the specimen (in mm).

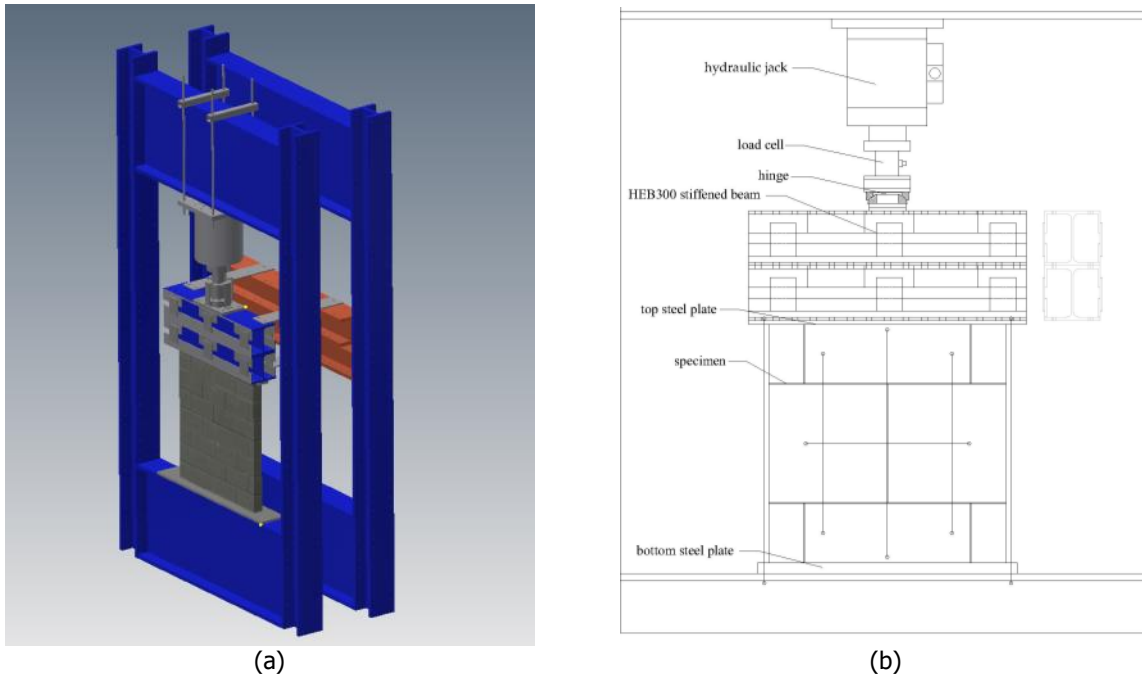


Figure 17 – Test setup: (a) 3D model; (b) drawing.

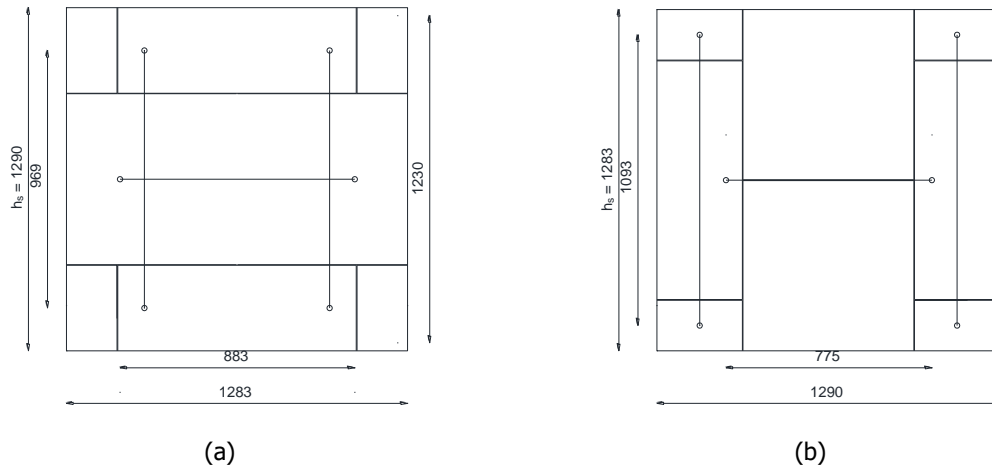


Figure 18 – Position of the LVDTs during the compression test on masonry: (a) vertical compression test; (b) horizontal compression test.

For the two configurations, three specimens were tested by applying a *monotonic loading* as prescribed by the EN 1052-1:1998 [10] (Figure 19a). Half of the expected maximum compression force is applied in three equal steps and was kept constant for 2 ± 1 min. Afterwards, the maximum stress reached monotonically. Subsequently, the test was continued to explore the post-peak behaviour. The load was applied with a rate of 0.015 mm/s to reach the peak stress in 15 to 30 min. The deformation and the force were registered, including the post-peak softening regime.

For the two configurations, three specimens were tested by applying a *cyclic loading* (Figure 19a). This loading scheme gives additional information regarding the loading-unloading behaviour. The cyclic loading was applied at approximately 1/4, 1/2 and 3/4 of the expected maximum strength. In every cycle the displacement was repeated three times. The load was applied with a rate of 0.05 mm/s to reach the peak stress in approximately 30 min. The deformation and the force were registered.

In the case of cyclic vertical compressive test, the specimens (TUD-MAT b/c/d), showed a strength higher than the capacity of the jack. In these cases, the loading procedure was modified as shown in Figure 19b:

- First, cyclic loading was applied at approximately 1/4, 1/2 and 3/4 of the expected maximum compressive strength (as prescribed by the protocol).
- Second, if the maximum capacity of the jack was reached, the load was kept constant for 2±1 minutes.
- Third, if after the application of the constant load failure did not occur, the specimen was unloaded and monotonic reloaded.

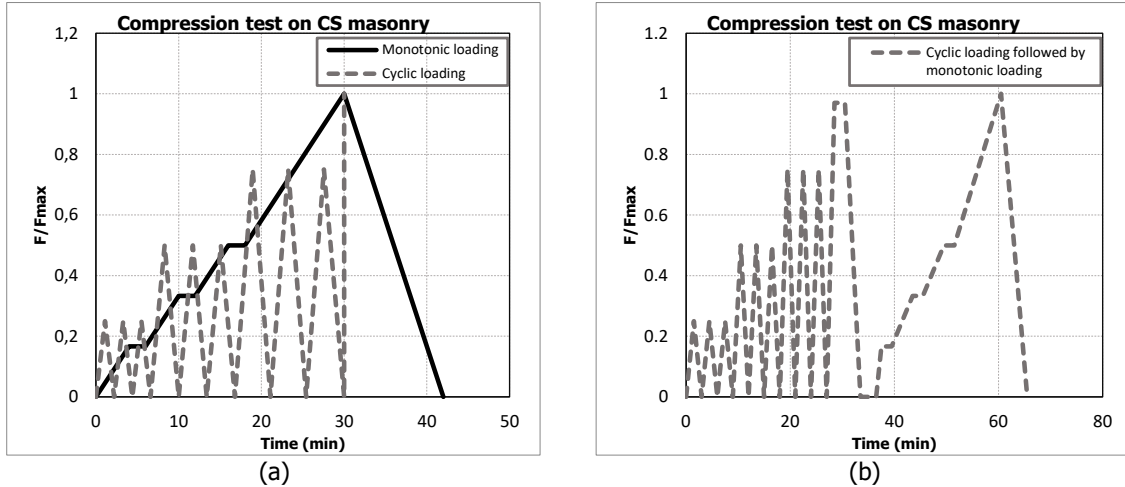


Figure 19 – Loading scheme for the calcium silicate element masonry: (a) monotonic and cyclic loading; (b) modified cyclic loading for the vertical compression.

8.2 Experimental results

Assuming that the stress is constant over the cross-section of the specimen, the compressive strength of masonry for the vertical, f'_m , and horizontal, $f'_{m,h}$, configuration can be determined as follows:

$$f'_m = \frac{F_{max}}{t_s l_s} \tag{9}$$

$$f'_{m,h} = \frac{F_{max}}{t_s h_s} \tag{10}$$

where F_{max} is the maximum load, l_s , h_s and t_s are the dimensions of the masonry specimen as built (Figure 18). During the test the displacements and the force were measured continuously allowing the determination of the stress-strain relationship along the loading direction, which was defined as normal direction. From this relation was possible to determine the elastic modulus of masonry. Three estimates of the elastic modulus were adopted (Figure 20a):

- $E_1 (E_{1,h})$ is the secant elastic modulus evaluated at 1/3 of the maximum stress;
- $E_2 (E_{2,h})$ is the secant elastic modulus evaluated at 1/10 of the maximum stress;
- $E_3 (E_{3,h})$ is the chord elastic modulus evaluated between 1/10 and 1/3 of the maximum stress.

The first estimate was consistent with the prescription of EN 1052-1:1998. The third estimate aimed to exclude the initial start-up of the stress-strain diagram, which would unrealistically affects the other two secant estimates with the initial lower slope.

The Poisson ratio ν is determined in the elastic phase as the ratio between the lateral strains, which are evaluated in the direction perpendicular to the loading one, and the normal strains (Figure 20b).

The displacement control procedure of the test allowed determining the post-peak behaviour of the material. The fracture energy in compression $G_{f-c} (G_{f-c,h})$ was determined as the area underneath the normal stress versus normal strain diagram, taking the height of the specimen into account. This concept was introduced by van Mier [11] for concrete material and subsequently applied to masonry by Lourenco [12]. In the case of cyclic loading, the envelope curve was considered for the calculation of the fracture energy.

The strain obtained by LVDTs' readings and by the plate's reading resulted similar in the post-peak phase. Consequently, the former were used to evaluate the pre-peak phase, while the latter were used to describe the post-peak phase, in which LVDTs may be detached from the specimen due to extensive cracking. The elastic modulus and the Poisson ratio were calculated on the basis of the LVDTs' readings, while the fracture energy was calculated on the basis of the LVDTs' readings in the pre-peak and the plate's reading in the post-peak phase.

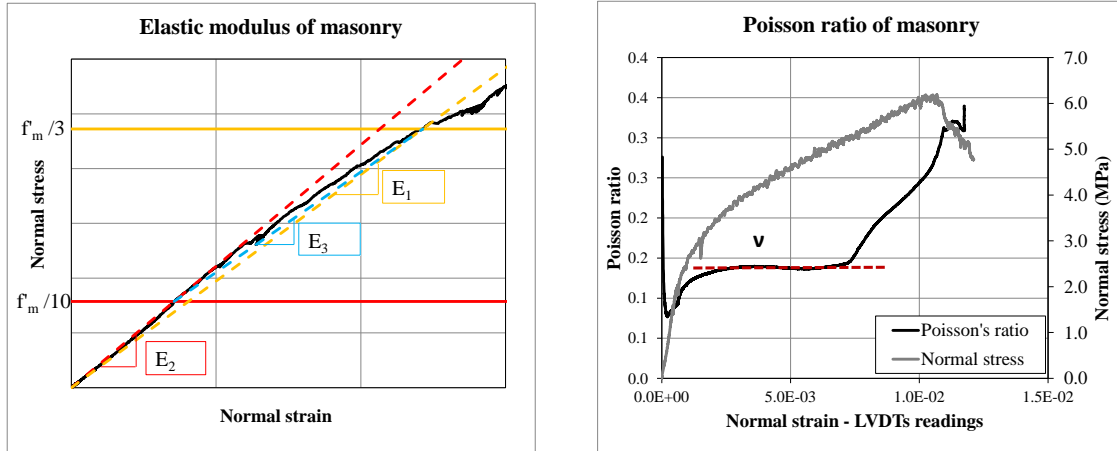


Figure 20 – Compression test on masonry: (a) three estimates of the elastic modulus; (b) evaluation of Poisson ratio.

Figure 21 and Figure 22 show the stress-strain diagram for calcium silicate element masonry under vertical and horizontal compression tests, respectively. The graphs refer to the normal direction that is defined as the one parallel to the loading direction.

For both configurations the stress-strain relationship in the normal direction showed a similar trend. The pre-peak stage was characterised by linear-elastic followed by a hardening behaviour until the peak. In this stage, the nonlinearity occurred at a stress level approximatively of 1/10 of the maximum stress. After the maximum stress was reached, a softening behaviour was observed. For both vertical and horizontal compression a brittle-failure was observed.

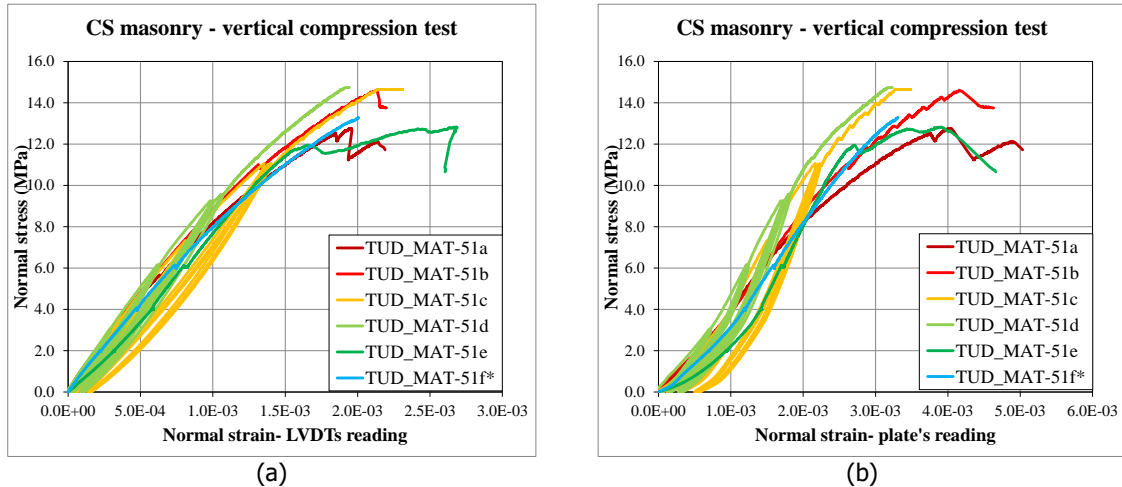


Figure 21 – Vertical compression tests on calcium silicate element masonry specimens: (a) normal strain obtained by LVDTs reading on the specimens; (b) normal strain obtained by LVDTs reading between the loading plates.

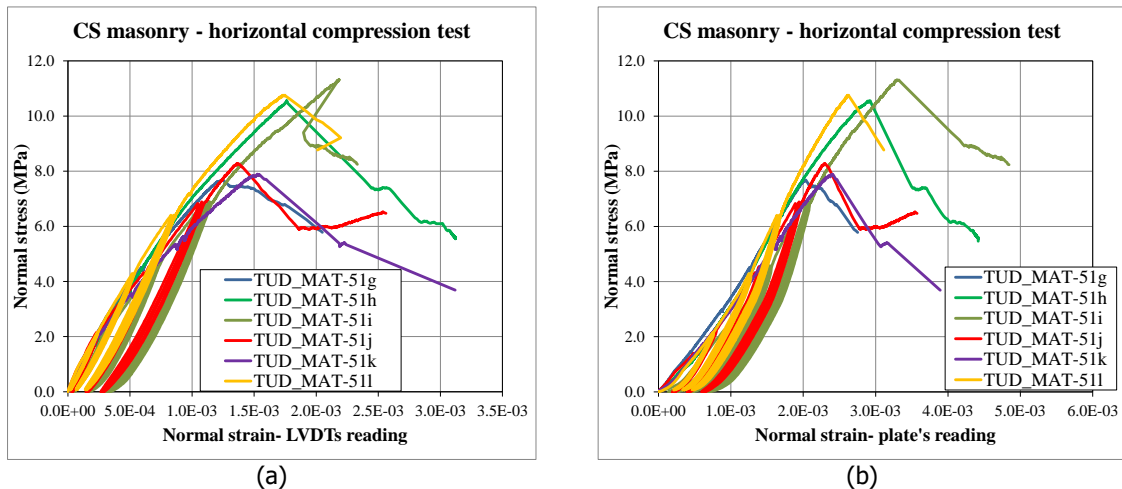


Figure 22 – Horizontal compression tests on calcium silicate element masonry specimens: (a) normal strain obtained by LVDTs readings on the specimens; (b) normal strain obtained by LVDTs reading between the loading plates.

Figure 23 and Figure 24 analyse the crack pattern in the two specimens tested under vertical and horizontal compression test, respectively.

In case of vertical compression test, the first cracks appeared on the middle joint, perpendicular to the loading direction (Figure 23a). As load increased the cracks mainly accumulated in the unit, causing spalling and delamination (Figure 23b). When maximum stress was reached, vertical cracks developed on the side joints, as well as along the thickness (Figure 23c).

In case of horizontal compression test, cracking and spalling started around the middle head joint, orthogonal to the applied load (Figure 24a). As load increased, the damage was concentrated in the bed joints, where smaller units were located (Figure 24b/c).

For both vertical and horizontal compression tests, cracking over the thickness of the specimen occurred resulting in one side being more damaged than the other.

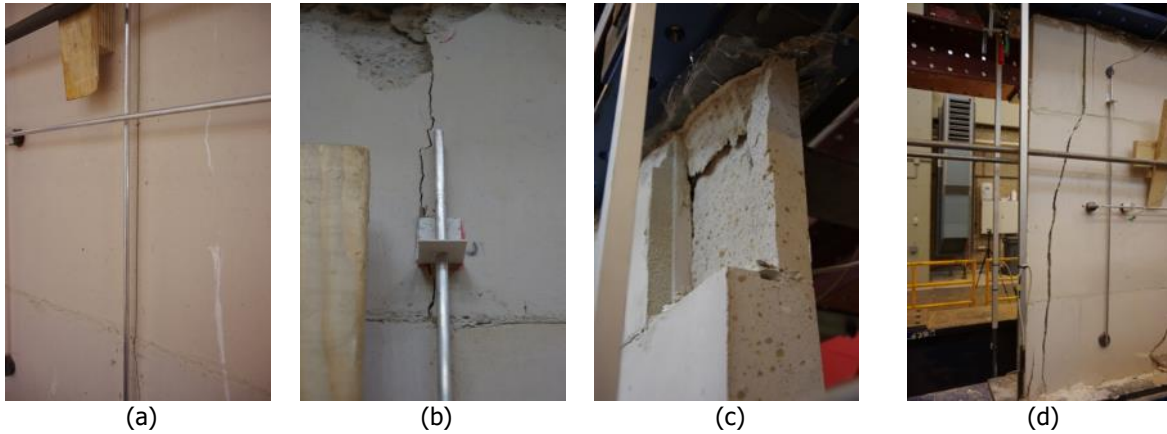


Figure 23 – Crack pattern of specimen TUD_MAT-51b tested under vertical compression test: (a) cracking of the central bed joint; (b) cracking and spalling; (c) splitting; (d) side failure.

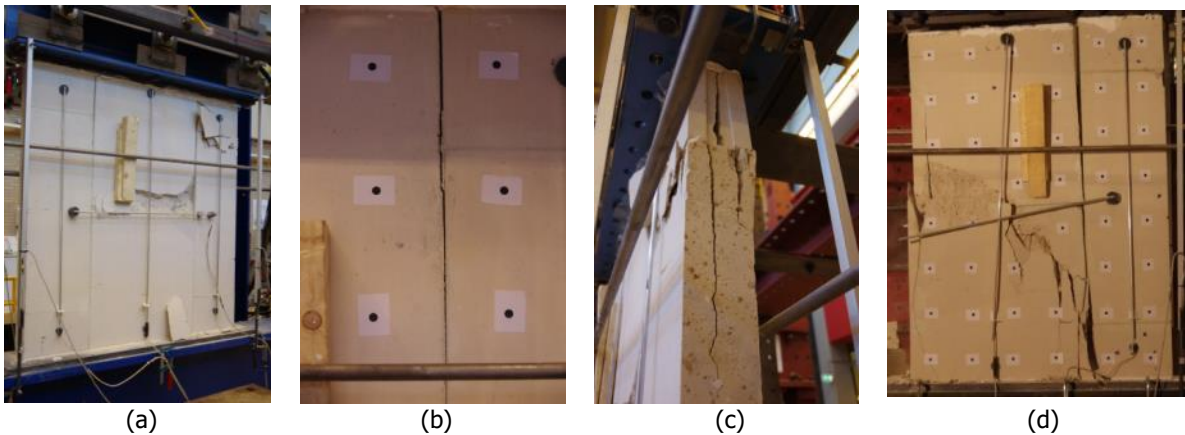


Figure 24 – Crack pattern of specimen TUD_MAT-51j tested under horizontal compression test: (a) cracking and spalling; (b) crack formation in bed joint; (c) splitting; (d) side failure

The main experimental results for the vertical compression tests are listed in Table 8. The specimens showed an average compressive strength of 13.9 MPa. The specimens subjected to cyclic tests showed a slightly higher value of the compressive strength with respect to the specimens tested under monotonic load. However, it should point out that this trend could be influenced by the testing procedure (Figure 19b). Considering the limited coefficient of variation reported (7%), all the results can be considered representative of the vertical compressive strength.

The secant elastic modulus E_1 , evaluated at 1/3 of the maximum stress, and the chord modulus E_3 provided a similar estimation, while the elastic modulus E_2 evaluated at 1/10 of the maximum stress provided higher values. This confirms the start of the non-linearity for lower values of normal stress. It should be reported that the specimen TUD_MAT-51f was unstable during the test thus the compressive strength could not be estimated; consequently, the Young’s moduli were evaluated by considering the average compressive strength.

The strain corresponding to peak stress and the fracture energy are reported as 2.01‰ and 20.9 N/mm, respectively.

Table 9 lists the main experimental results for the calcium silicate element masonry specimens subjected to horizontal compression test. The specimens showed an average horizontal compressive strength of 9.4 MPa. There is no clear trend where the specimens subjected to cyclic loading showing higher compressive strength than those specimens subjected to monotonic loading.

The secant elastic modulus $E_{1,h}$, evaluated at 1/3 of the maximum stress, and the chord modulus $E_{3,h}$ provided a similar estimation, while the elastic modulus $E_{2,h}$ evaluated at 1/10 of the maximum stress provided higher values. This confirms the start of the non-linearity for lower values of normal stress.

The strain corresponding to peak stress and the fracture energy are reported as 1.58‰ and 12.8 N/mm, respectively.

Table 10 lists the main experimental results for the calcium silicate element masonry specimens. Figure 25 and Figure 26 show the results through the histogram. The calcium silicate element masonry showed an orthotropic behaviour, having a higher compressive strength in the direction perpendicular to the bed joints ($f'_m / f'_{m,h} = 1.48$). Similarly, a higher ratio was observed in terms of fracture energy ($G_{f-c} / G_{f-c,h} = 1.63$) and strain at peak ($\epsilon_p / \epsilon_{p,h} = 1.3$) in the direction perpendicular to the bed joints. On the contrary, the stiffness obtained in both configurations was almost the same ($E_1 / E_{1,h} = 1.0$, $E_3 / E_{3,h} = 1.1$).

By analysing the crack pattern, it was possible to conclude that when the calcium silicate masonry specimen was rotated and the direction of the bed joints coincided with the loading direction, the damage mainly started in the unit-mortar interfaces of bed joints. On the contrary, when the load was applied perpendicular to the bed joints, the cracking and eventual failure concentrated on the head joints, see Figure 23 and Figure 24.

Table 8 – Vertical compression test results on calcium silicate element masonry specimens.

Specimen name	Test type	f'_m	E_1	E_2	E_3	ϵ_p	G_{f-c}
		MPa	MPa	MPa	MPa	‰	N/mm
TUD_MAT-51a	monotonic	12.77	9698	12389	8748	1.89	18.48
TUD_MAT-51e	monotonic	12.83	6897	6079	7394	2.14	29.36
TUD_MAT-51f	monotonic	-	10665	11845	10160	1.94	-
TUD_MAT-51b	cyclic	14.61	9399	10263	9019	1.71	23.26
TUD_MAT-51c	cyclic+ monotonic	14.64	6654	6626	6669	2.68	17.46
TUD_MAT-51d	cyclic+ monotonic	14.79	8031	8337	7887	1.68	15.91
Average		13.93	8557	9256	8313	2.01	20.9
Standard deviation		1.03	1619	2660	1251	0.37	5.47
Coefficient of variation		0.07	0.19	0.29	0.15	0.19	0.26

Table 9 – Horizontal compression test results on calcium silicate element masonry specimens.

Specimen name	Test type	$f'_{m,h}$	$E_{1,h}$	$E_{2,h}$	$E_{3,h}$	$\epsilon_{p,h}$	$G_{f-c,h}$
		MPa	MPa	MPa	MPa	‰	N/mm
TUD_MAT-51g	monotonic	7.69	9797	11073	9264	1.11	6.42
TUD_MAT-51h	monotonic	10.56	8172	8666	7945	1.73	13.35
TUD_MAT-51i	cyclic	11.32	6067	8655	5278	2.20	18.39
TUD_MAT-51j	cyclic	8.28	9968	12736	8992	1.25	15.03
TUD_MAT-51k	monotonic	7.89	7749	11554	6653	1.52	9.06
TUD_MAT-51l	cyclic	10.76	8740	10463	8075	1.71	14.47
Average		9.42	8416	10524	7701	1.58	12.8
Standard deviation		1.63	1445	1625	1502	0.39	4.34
Coefficient of variation		0.17	0.17	0.15	0.19	0.24	0.34

Table 10 – Orthotropic behaviour of calcium silicate element masonry.

Specimen name	f'_m	E_1	E_2	E_3	ϵ_p	G_{f-c}
	$f'_{m,h}$	$E_{1,h}$	$E_{2,h}$	$E_{3,h}$	$\epsilon_{p,h}$	$G_{f-c,h}$
	MPa	MPa	MPa	MPa	‰	N/mm
Vertical configuration	13.93	8557	9256	8313	2.01	20.9
Horizontal configuration	9.42	8416	10524	7701	1.58	12.8
Ratio Vertical/Horizontal	1.48	1.02	0.88	1.08	1.27	1.63

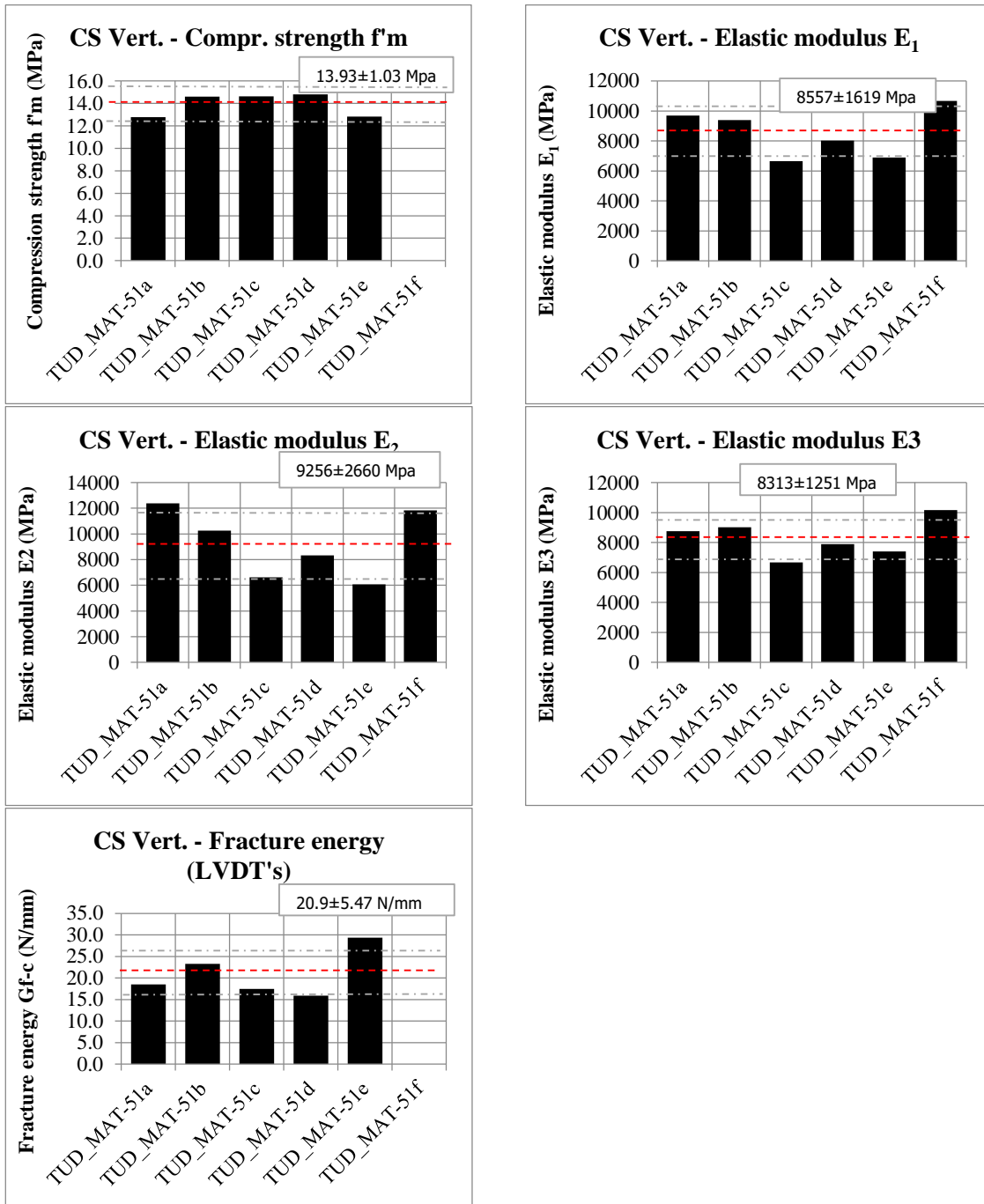


Figure 25 - Vertical compression tests on calcium silicate element masonry specimens: histogram representation.

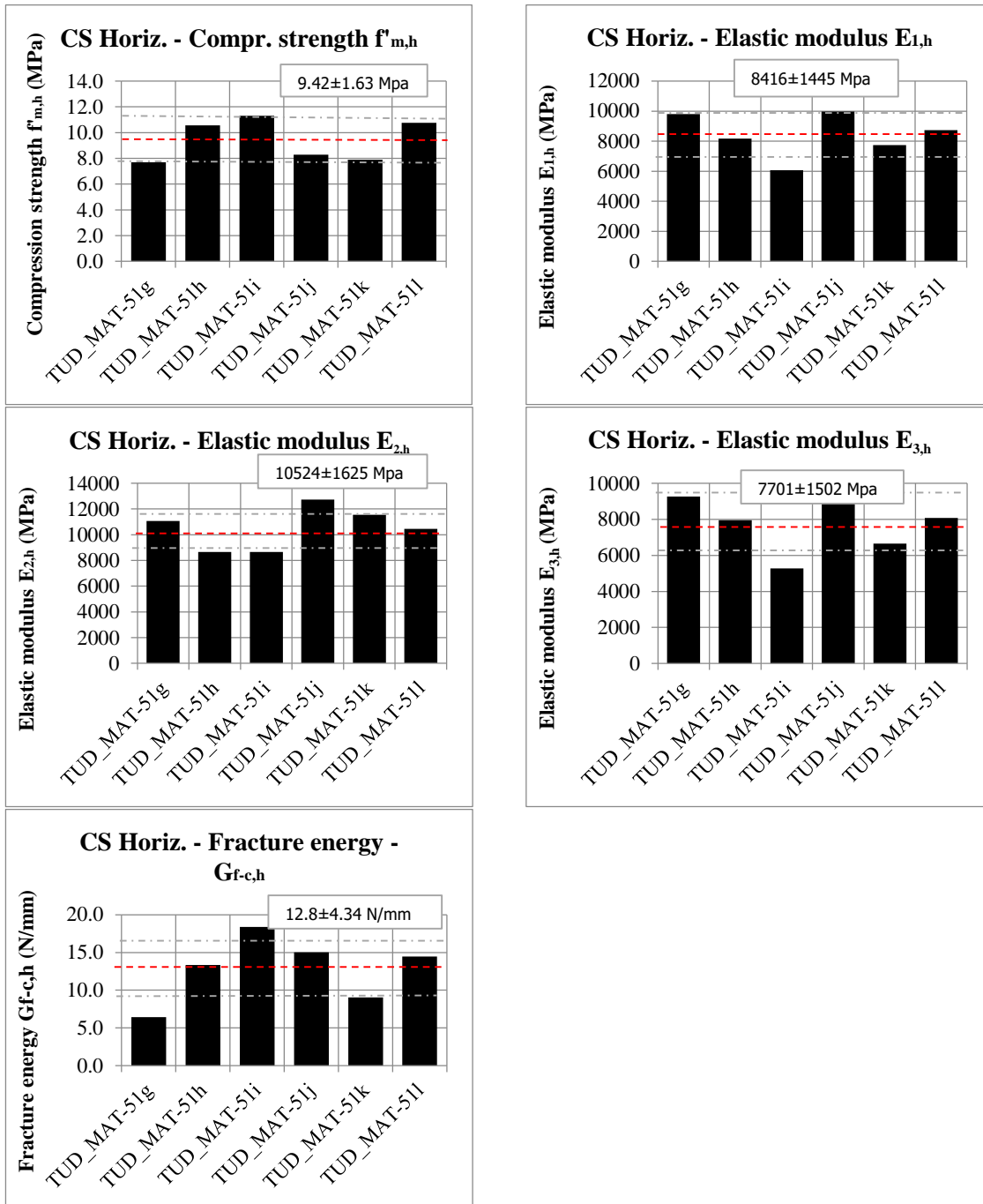


Figure 26 - Horizontal compression tests on calcium silicate element masonry specimens: histogram representation.

9 Flexural strength of masonry

The flexural strength of masonry was determined for three configurations:

- Four-point bending test with the moment vector parallel to the bed joints and in the plane of the wall, which generates a plane of failure parallel to the bed joints (denoted as vertical out-of-plane bending test OOP1);
- Four-point bending with the moment vector orthogonal to the bed joints and in the plane of the wall, which generates a plane of failure perpendicular to the bed joints (denoted as horizontal out-of-plane bending test OOP2);
- Four-point bending with the moment vector orthogonal to plane of the wall (denoted as in-plane vertical bending test IP).

The first two tests were performed in agreement with EN 1052-2:1999 [13], while the third one was a non-standard test.

9.1 Testing procedure

The masonry specimens tested with the moment vector in the plane of the wallets were designed in agreement with EN 1052-2:1999 [13]. Table 11 provides an overview of dimensions of the specimens tested. The masonry type, the dimensions and the distance between the bearing supports d_1 and loading supports d_2 are listed. More information regarding the size of the specimens can be found in Ref.[1].

Table 11 – Overview of specimens for bending tests.

Test type	Specimen name	l_s (mm)	h_s (mm)	d_2 (mm)	d_1 (mm)
Bending test with moment vector parallel to the bed joints and in the plane of the wall (OOP1)	TUD_MAT52	1350	1930	950	1750
Bending test with moment vector orthogonal to the bed joints and in the plane of the wall (OOP2)	TUD_MAT53	2250	1290	950	1750
Bending test with moment vector orthogonal to the bed joints and in the plane of the wall (IP)	TUD_MAT54	2247	645	950	1750

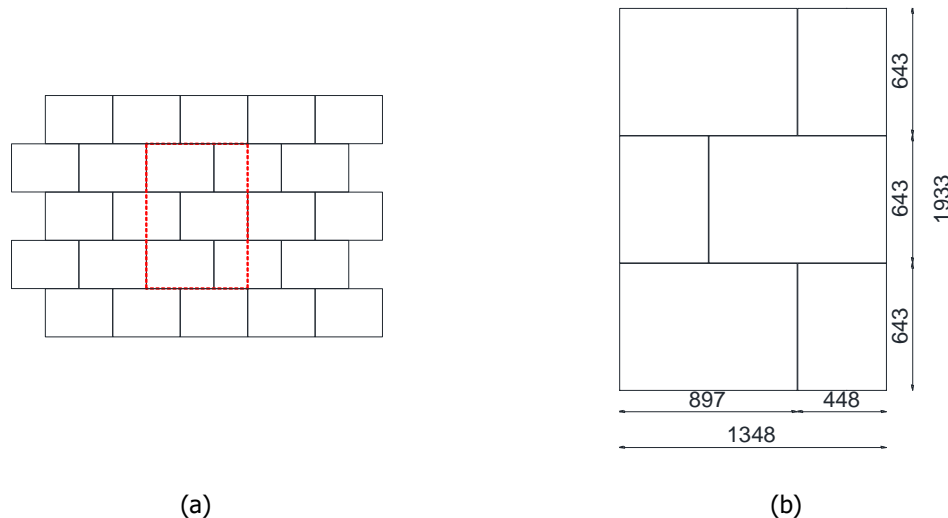


Figure 27 – Vertical out-of-plane bending test (OOP1): (a) tested portion; (b) dimensions of the specimen.

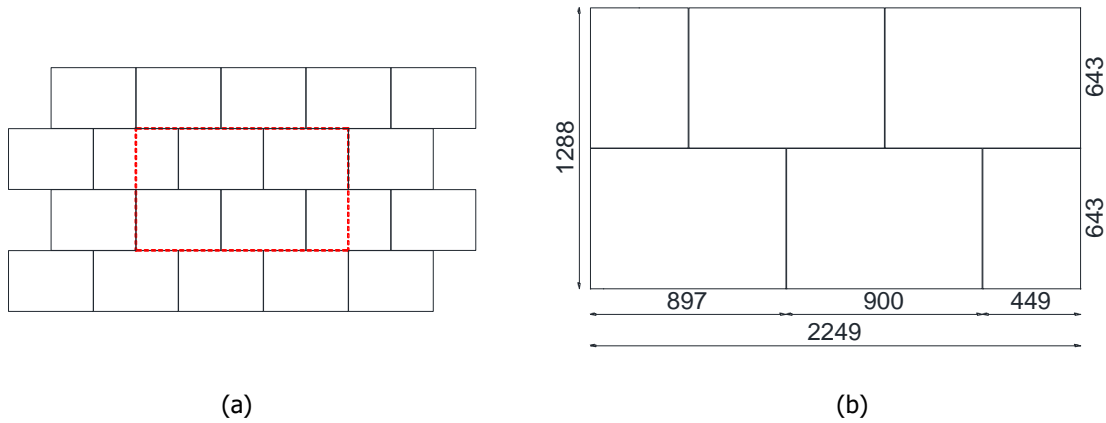


Figure 28 - Horizontal out-of-plane bending test (OOP2): (a) tested portion; (b) dimensions of the specimen.

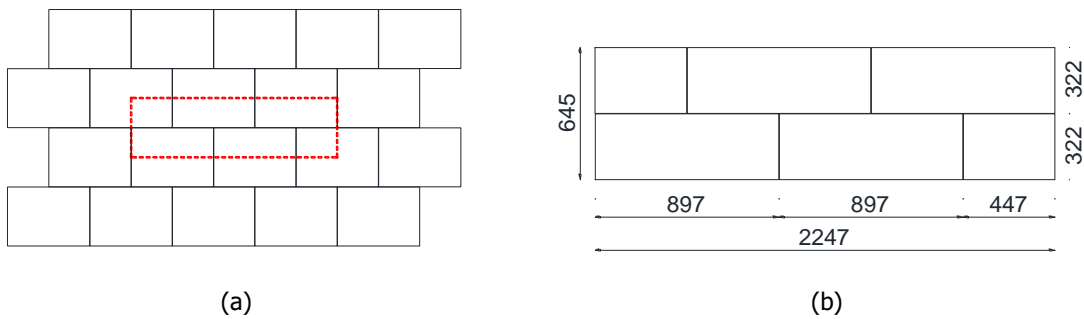


Figure 29 – In-plane bending test (IP): (a) tested portion; (b) dimensions of the specimen.

In the current testing campaign, a new testing set-up for the out-of-plane bending tests was designed, as shown in Figure 30. In the improved set-up, the specimens were placed vertically and loaded in such a way that the bending axis was always horizontal. Consequently, the contribution of the masonry self-weight was excluded. The load was applied via cylindrical roller bearings mounted to steel hollow profiles with springs which enabled them to easily move. At the base, the specimen was supported by a steel plate positioned on top of flat ball bearings. A counterweight was used to minimise the friction forces between the loading support and the specimen. The bearing rollers were mounted to the test rig with springs. The distance between the loading, d_z , and bearing rollers, d_i , is chosen equal to 0.5 (Table 11).

The load was applied in displacement control by a spherical joint attached to a hydraulic jack with 100 kN capacity. The applied load was recorded from the load cell attached to the hydraulic jack. For each side, a maximum of five LVDTs was attached to measure the vertical and horizontal displacements in the constant moment zone (Figure 30a). The LVDTs had a measuring range of 10 mm with an accuracy of 0.1%. Apart from the test set-up, the measuring system was also improved, by which a better understanding on the post-peak behaviour of masonry could be gained. In this view, four vertical LVDTs were installed on the back face of the specimen to measure the cracks opening (Figure 30b). The average of readings of these LVDTs was used as a parameter to control the applied load.

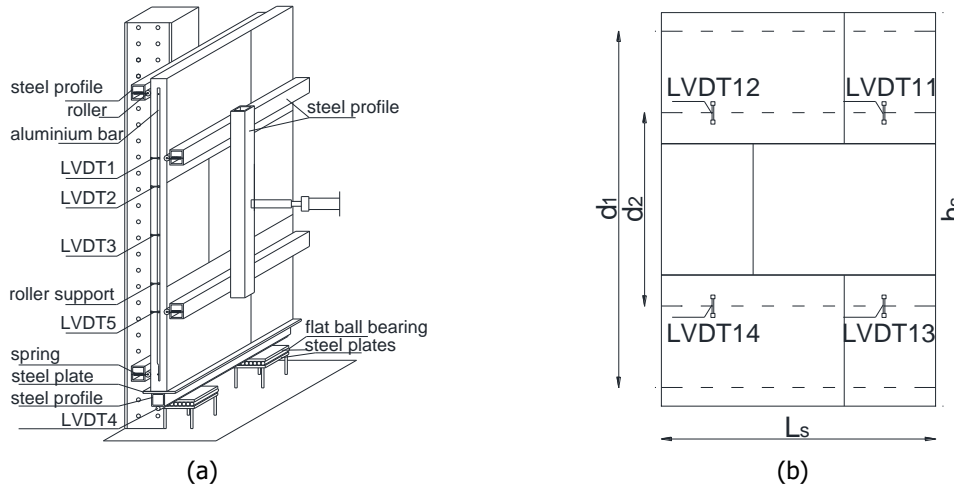


Figure 30 – Out-of-plane bending: (a) testing set-up; (b) average of LVDTs reading used as control parameter.

Figure 31 shows the in-plane bending test set-up. The load was applied in displacement control by a spherical joint attached to a hydraulic jack with 100 kN capacity. The applied load was recorded from the load cell attached to the hydraulic jack. The vertical displacement of the specimen in the constant moment zone was measured using five vertical LVDTs on each side. In addition, the crack opening was measured using the horizontal LVDTs; one on each side. The average of readings of two horizontal LVDTs was used as a parameter to control the applied load.

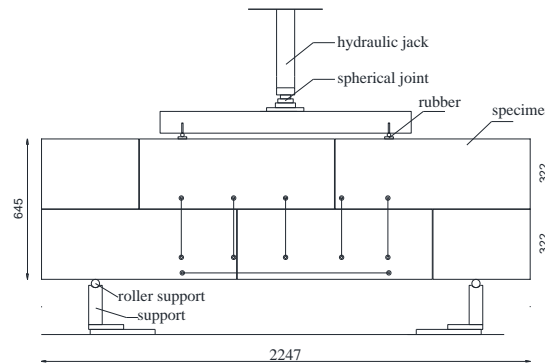


Figure 31 – Set-up for the in-plane bending test (IP).

9.2 Experimental results

The flexural strength of the out-of-plane tests can be determined as follows:

$$f_{x1} = \frac{3F_{\max} d_3}{l_s t_s^2} \quad (11)$$

$$f_{x2} = \frac{3F_{\max} d_3}{h_s t_s^2} \quad (12)$$

where F_{\max} is the maximum load at failure, d_3 (=400 mm) is the distance between the loading and the bearing support, l_s is the length of masonry specimen as built, h_s is the height of masonry specimen as built and, t_s is the thickness of masonry specimen as built.

Assuming a linear stress distribution over the height of the specimen's cross-section, the elastic modulus of the masonry from out-of-plane bending test can be determined as follows:

$$E_{f_{x,i}} = \frac{\frac{F_{el}}{2} \times \frac{(d_1 - d_2)}{2} \times (3d_1^2 - 4(\frac{(d_1 - d_2)^2}{2}))}{24v_{el}I}} \quad (13)$$

where F_{el} and v_{el} are the load and mid-span vertical displacement in the linear elastic stage, respectively, I is the moment of inertia of the masonry along the cross-section, d_1 and d_2 are the distances between the loading and bearing loading, respectively. The elastic modulus was calculated between 1/10 and 1/3 of the maximum force.

The concept of fracture energy associated with tensile cracking was applied to masonry by Van der Pluijm [14]. Thanks to the improved test set-up, the post-peak behaviour could be recorded during the bending test and an estimation of the fracture energy can be provided. The fracture energy for the vertical out-of-plane bending, G_{fx1} , and horizontal out-of-plane bending, G_{fx2} , is determined considering the area underneath the curve relating the load and the deflection measured in correspondence of the loading points (Figure 32). The estimation takes into account the cross-section of the specimen.

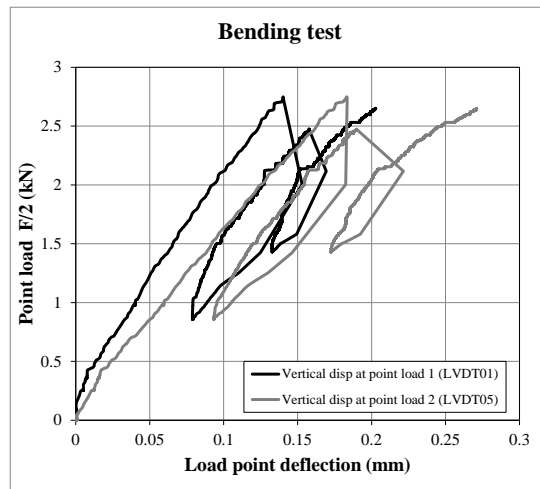


Figure 32 – Force versus displacement of the point-loads for CS element masonry specimens subjected to out-of-plane bending tests used to calculate the fracture energy in bending.

The flexural strength of the in-plane tests f_{x3} can be determined as follows:

$$f_{x3} = \frac{M_{max}}{W} = \frac{(F_{max} d_3 / 2 + p d_1^2 / 8)}{W} \quad (14)$$

where M_{max} is the maximum bending moment, F_{max} is the maximum load at failure, d_3 is the distance between the loading and the bearing support, d_1 is the distance between the bearing support, p is the masonry self-weight uniform load (calculated assuming a density of 1800 kg/m³ obtained from the bond-wrench test) and W is the section modulus.

The Young's modulus obtained from the in-plane bending test can be calculated from the moment-curvature curve. The curvature is calculated from the horizontal LVDT's readings. The Young's modulus can be determined as follows:

$$E_{f_{x3}} = \frac{M}{I\kappa} \quad (15)$$

where M is the bending moment in the linear elastic stage, I is the moment of inertia of the masonry unit along the cross-section and κ is curvature determined as the strain calculated from the horizontal LVDTs readings in the linear elastic stage divided by the vertical distance of the LVDTs from the neutral axis.

Figure 33 shows the force displacement curve for the calcium silicate element masonry specimens subjected to out-of-plane bending tests. The mid-span displacement has been calculated from the readings of the LVDTs. Figure 34 shows the moment-curvature curve for the calcium silicate element masonry specimens subjected to the in-plane bending tests.

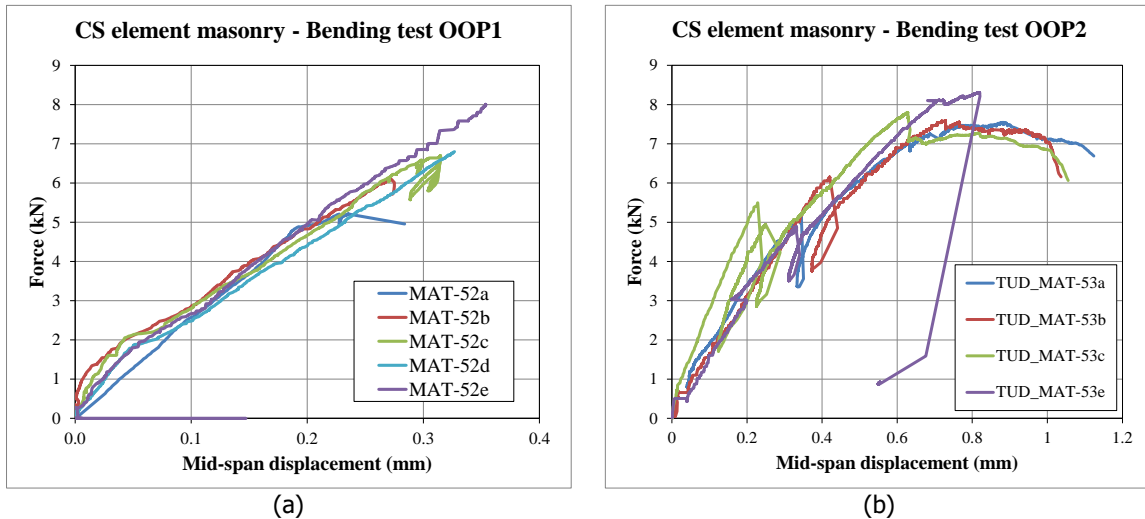


Figure 33 – Force-displacement curve for calcium silicate element masonry specimens subjected to: (a) vertical out-of-plane bending test; (b) horizontal out-of-plane bending test.

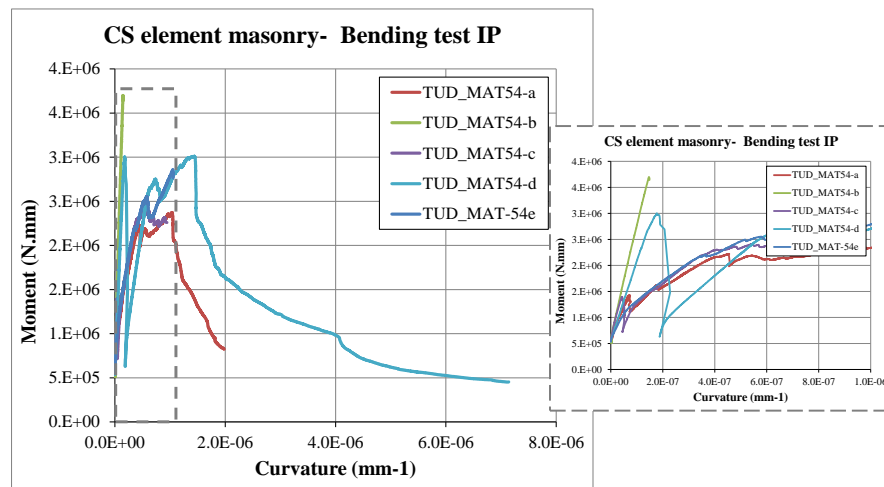


Figure 34 – Moment-curvature for calcium silicate element masonry specimens subjected to in-plane bending test.

The crack pattern for each bending test is shown in Figure 35 to Figure 37.

For the vertical out-of-plane test, the specimens cracked in one bed joint located in the constant moment zone (see Figure 35), either in the lower bed joint (TUD_MAT-52b and TUD_MAT-52d) or in the upper joint (TUD_MAT-52a, TUD_MAT-52c and TUD_MAT-52e). A brittle failure mechanism was observed.

In the case of horizontal out-of-plane bending tests, alternating crack appeared running through the head joints and bed joints. In addition, splitting of the unit was reported, except for one sample (TUD_MAT-53e). A brittle failure mechanism was observed.

For the in-plane bending test a brittle or a quasi-brittle behaviour was reported. The cracking occurred in both bed and head joints in the constant moment zone, creating a stepwise pattern. For sample TUD_MAT-54d splitting of the unit was reported, which could be related to weakness of the specimen (Figure 38). As can be seen in Figure 34, a sudden drop in force for this specimen in the pre-peak phase was observed.

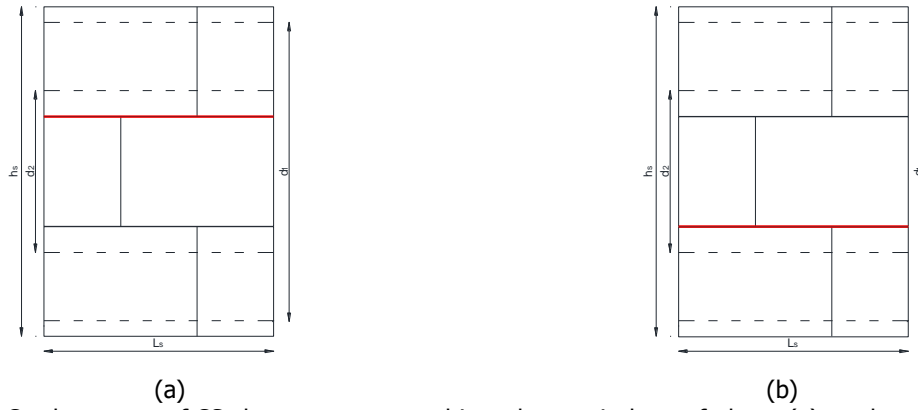


Figure 35 – Crack patterns of CS element masonry subjected to vertical out-of-plane: (a) crack on the top joint; (b) crack on the bottom joint.

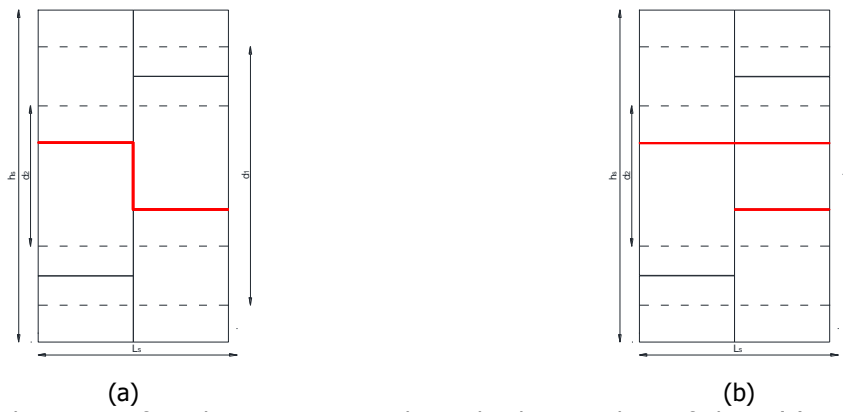


Figure 36 – Crack patterns of CS element masonry subjected to horizontal out-of-plane: (a) stepwise crack; (b) stepwise crack and splitting of unit;

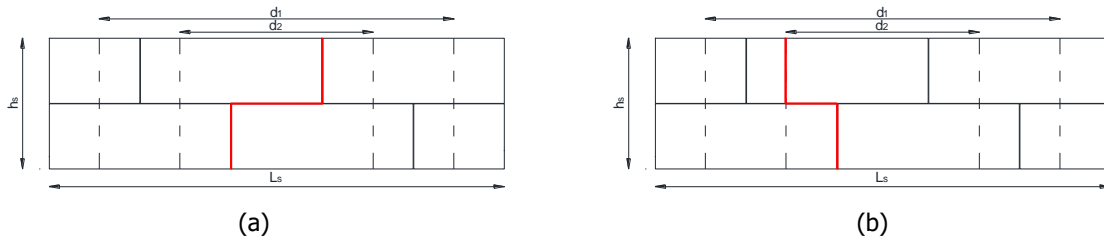


Figure 37 – Crack patterns of CS element masonry subjected to in-plane bending: (a) stepwise crack alternating through joints; (b) splitting of the units and stepwise crack through joints.

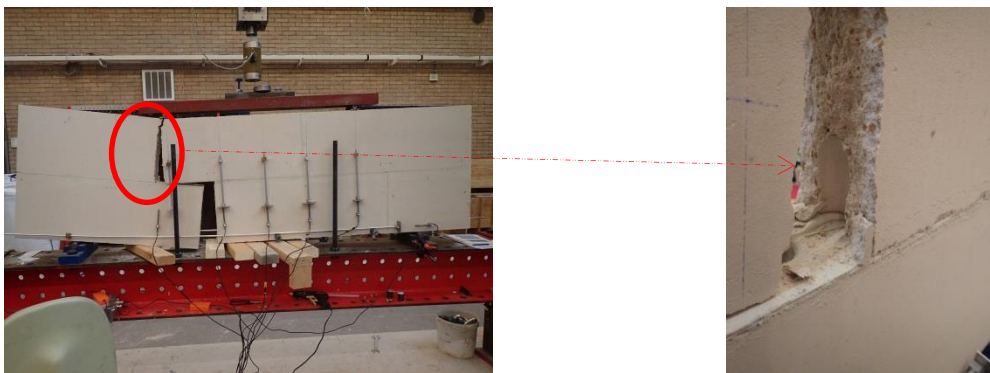


Figure 38 - Crack pattern of specimen TUD_MAT-54d subjected to in-plane bending test.

Table 12 lists the out-of-plane and in-plane bending properties, while Figure 39 shows the flexural strength values of by adopting histogram representation. The calcium silicate masonry showed an orthotropic behaviour. The horizontal out-of-plane flexural strength resulted approximately 1.3 times higher values than the vertical out-of-plane flexural strength ($f_{x2} / f_{x1} = 1.3$). The in-plane vertical strength was lower than those of the vertical out-of-plane flexural strength ($f_{x3} / f_{x1} = 0.71$). Out-of-plane bending tests show high value of elastic modulus, while for in-plane bending tests the elastic modulus is in the same range of the one estimated with compression tests. The fracture energy obtained from horizontal out-of-plane tests results approximately 5 times higher than the one obtained from vertical out-of-plane bending tests.

Table 12 – Bending properties of calcium silicate element masonry.

Specimen name	f_{x1}	E_{fx1}	G_{fx1}	Specimen name	f_{x2}	E_{fx2}	G_{fx2}	Specimen name	f_{x3}	E_{fx3}
	MPa	MPa	N/mm		MPa	MPa	N/mm		MPa	MPa
MAT-52a	0.46	16740	0.0046	MAT-53a	0.70	10816	0.058	MAT-54a	0.34	6651
MAT-52b	0.54	18865	0.0082	MAT-53b	0.71	9871	0.039	MAT-54b	0.53	9811
MAT-52c	0.60	21291	0.0102	MAT-53c	0.73	14044	0.048	MAT-54c	0.34	8066
MAT-52d	0.60	17160	0.0098	MAT-53d*	-	-	-	MAT-54d	0.43	6913
MAT-52e	0.71	14045	0.0082	MAT-53e	0.77	11724	0.028	MAT-54e	0.41	3798
Avg.	0.58	17620	0.0082	Avg.	0.73	11614	0.0433	Avg.	0.41	7048
C.o.V.	0.08	2400	0.0020	C.o.V.	0.03	1549	0.0112	C.o.V.	0.07	1970
St. dev.	0.14	0.14	0.24	St. dev.	0.04	0.13	0.26	St. dev.	0.17	0.28
				f_{x2} / f_{x1}	1.26			f_{x3} / f_{x1}	0.7	

*Unreliable results due to the technical problem during the test.

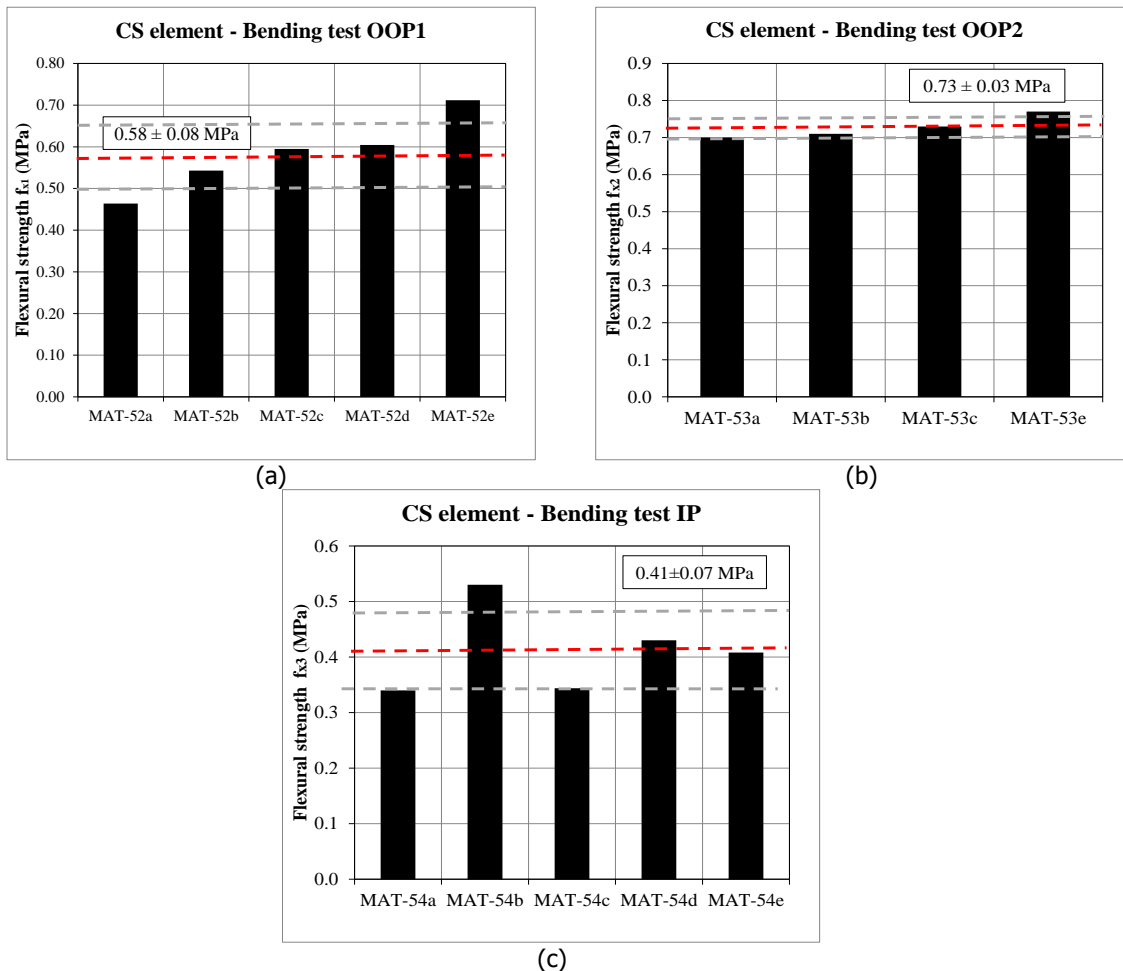


Figure 39 – Histogram representation of the flexural strength values of calcium silicate element masonry: (a) vertical out-of-plane bending test; (b) horizontal out-of-plane bending; (c) in-plane bending.

10 Bond strength of masonry

The bond strength between masonry unit and mortar was determined in agreement with the bond wrench test proposed by EN 1052-5:2002 [15].

10.1 Testing procedure

The bond wrench test was performed on two bonded portions of the elements that were sawn-cut from the top and bottom of single element. The surfaces bonded together for testing are the original ones and not the cut faces. Each cut portion was 224x60x100-mm. More information regarding the size of the specimens can be found on Ref. [1].

As mentioned in Section 3, for transportation purpose, two holes are presents on the top side of the element. To investigate the possible effect of the holes on the bond strength, two types of samples were adopted; with holes (indicated as type I) and without hole (indicated as Type II). Totally, 11 couplets for each type were tested.

The set-up improved in the current campaign is shown in Figure 40b. The specimen is rigidly held by a support frame that holds the specimen in accordance with EN 1052-5:2005 [15]. A clamp, with a lever attached, was applied to the masonry unit above the tested. The lever was used to apply a bending moment to the brick-mortar interface. The load was applied by a jack operated manually and a load cell attached to the jack measures the applied force. Therefore, the improved set-up provides the possibility for recording the applied load continuously and the better control of the load.



Figure 40 – Bond wrench tests: (a) couplets adopted for the test; (b) improved bond wrench set-up.

10.2 Experimental results

The bond wrench strength f_w is calculated on the assumption that the stress distribution is linear over the width of the top masonry unit [15]:

$$f_w = \frac{F_1 e_1 + F_2 e_2 - \frac{2}{3} t_u \left(F_1 + F_2 + \frac{F_3}{4} \right)}{l_j w_j^2 / 6} \quad (16)$$

where F_1 is the failure load measured and applied by the jack. F_2 is the normal force as a result of the weight of the bond wrench apparatus. F_3 is the weight of the masonry unit pulled off the specimen, including the weight of adherent mortar. Furthermore, e_1 is the distance from the applied load to the tension face of the specimen, e_2 is the distance from the centre of gravity of the clamp to the tension face of the specimen, l_j is the mean length of the bed joint and w_j is the mean width of the bed joint. The set-up and the definition of the various quantities are shown in Figure 41.

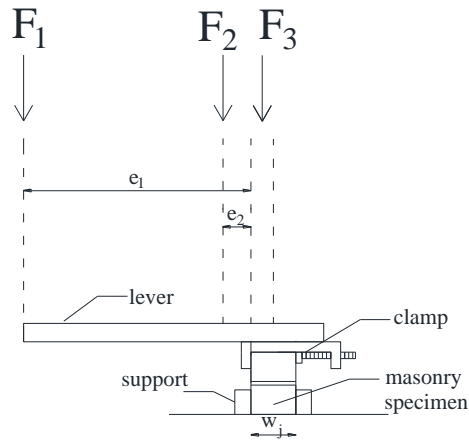


Figure 41 - Test set-up for the bond wrench test.

Figure 42 reports the classification of the type of failures according to [15], while Figure 43 shows the observed failure mechanisms.

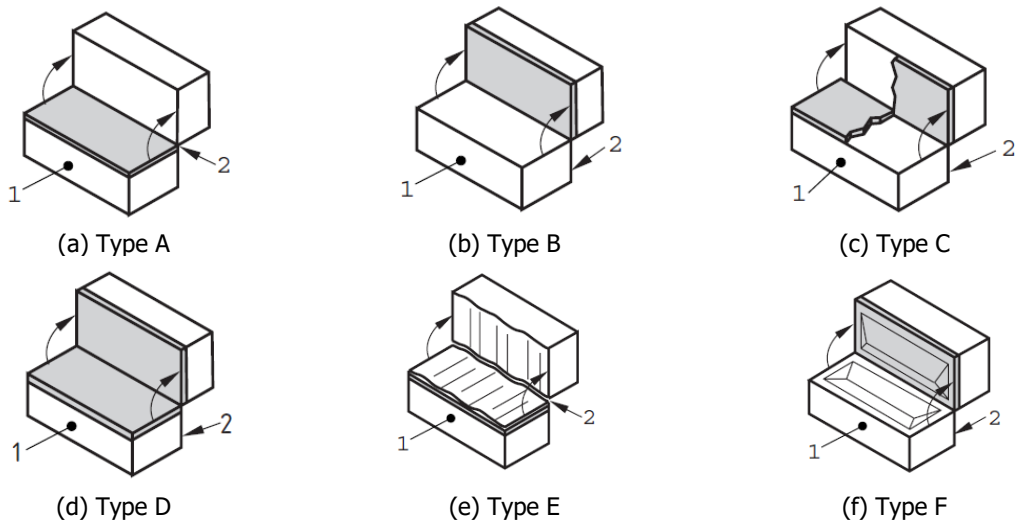


Figure 42 - Classification of failure modes in agreement with EN-1052-5:2005 (1 tension face, 2 compression face).



Figure 43 - Observed failure mechanisms: (a) type B for sample type I (with hole); (b) type A and, (c) type B for sample type II (without hole).

Figure 44 shows the applied load (F_t) versus time. The specimens showed brittle behaviour.

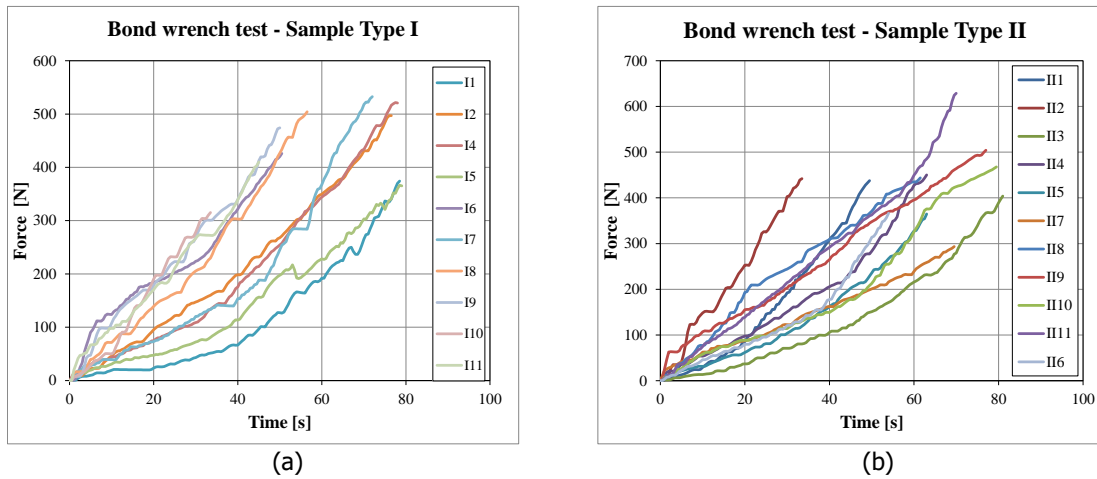


Figure 44 – Time versus force applied by manually controlled jack: (a) sample type I (with hole); (b) sample type II (without hole).

Table 13 – Bond strength of calcium silicate element masonry.

Specimen Name	l_j	w_j	F_3	F_1	f_w	Failure mode
	mm	mm	N	N	MPa	
MAT-55 I-1*	221	99	22.95	374.27	0.45	Failure happened before in the bottom brick
MAT-55 I-2	222	100	24.47	497.16	0.58	B
MAT-55 I-3	222	100	24.47	785.57	0.92	Failure happened before in the bottom brick
MAT-55 I-4*	221	99	24.47	521.59	0.62	B
MAT-55 I-5	217	99	23.44	366.35	0.45	B
MAT-55 I-6	222	99	24.12	496.74	0.59	B
MAT-55 I-7	218	99	22.50	532.78	0.65	B
MAT-55 I-8	220	98	24.56	504.19	0.62	B
MAT-55 I-9	216	99	23.04	474.09	0.58	B/C type failure
MAT-55 I-10	216	98	25.54	315.18	0.39	B
MAT-55 I-11	215	99	23.58	410.07	0.50	B
MAT-55 II-1	221	100	23.39	437.73	0.51	B
MAT-55 II-2	221	98	23.63	442.11	0.54	B
MAT-55 II-3	221	99	24.22	403.77	0.48	B
MAT-55 II-4	217	99	23.34	511.30	0.62	B
MAT-55 II-5	219	99	23.29	495.93	0.60	B
MAT-55 II-6	218	100	24.47	366.49	0.43	A
MAT-55 II-7	222	100	24.81	293.54	0.34	A
MAT-55 II-8	217	100	24.12	443.71	0.53	B
MAT-55 II-9	221	99	23.00	504.12	0.60	Irregular B type failure
MAT-55 II-10	221	98	23.63	467.58	0.57	Irregular B type failure
MAT-55 II-11	221	100	24.07	628.74	0.74	
Average					0.55	
Standard deviation					0.09	
Coefficient of variation					0.17	
f_{k1}/f_w					1.05	

* excluded from the average due to crushing of the lower unit prior to failure in the brick-mortar interface

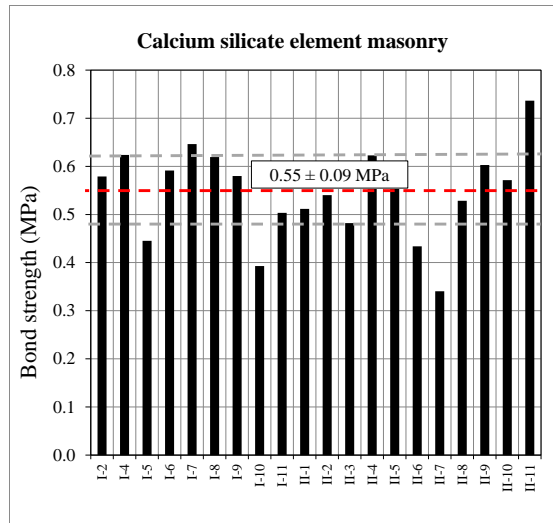


Figure 45 – Bond strength values of calcium silicate element masonry: histogram representation.

Table 13 lists the results of the calcium silicate element masonry for both type of specimens and Figure 45 show the histogram representation. The average bond strength for type I and type II was obtained as 0.55 MPa and 0.54 MPa, respectively. It can be concluded that the presence of the hole did not have effect on the bond strength. As a result, the average results of the two types of specimens, with and without hole, are reported in Table 13.

From a physical point of view, it may be expected that there is a correlation between the flexural bond tensile strength, f_{wv} and flexural masonry strength. This correlation depends on loading direction so that the crack plane occurs along the brick to mortar interface in the bed joint plane, f_{xL} . A ratio approximately equal to 1 is found between the flexural bond tensile strength, f_{wv} and the vertical out-of-plane strength, f_{xL} .

11 Shear properties of masonry

The initial shear properties of masonry were determined in agreement with EN 1052-3:2002 [16]. However, a displacement-control procedure was used, instead of the prescribed force control procedure.

11.1 Testing procedure

The couplet specimens were composed of two sawn-cut parts extracted from the top and bottom of one single calcium silicate element: one wide part having dimensions 300x100x100-mm and one narrow part having dimensions 100x100x100-mm (Figure 46a). In total, eleven specimens were tested. The surfaces bonded together were the original ones and not the cut faces. A layer of gypsum 10 mm thick was applied to the external faces of the specimens allowing a better distribution of the stresses on the contact surfaces. More detailed information regarding the dimensions of the samples can be found on Ref.[1].

Figure 46b shows the tests set-up used. The distance between the two supports (steel rollers) was chosen in agreement with EN 1052-3:2002 [16]. During the test, the specimen was rotated of 90 degree with respect to the casting position (Figure 46). The specimen was kept under constant lateral pre-compression, while a shear load was applied near the joint. Three different levels of pre-compression were investigated. Being the compressive strength of the masonry unit greater than 10 N/mm² [16], the pre-compression stresses applied were 0.2, 0.6 and 1.0 N/mm². Minimum three samples for each pre-compression level were tested.

Two independently operated jacks were required to apply the shear and pre-compressive load. The shear load acts in a vertical direction using a displacement controlled apparatus. The apparatus has a 100 kN jack and a spherical joint. The displacement increased at a rate of 0.005 mm/s. The pre-compressive load was applied perpendicular to the bed joint plane by a manually operated hydraulic jack. The horizontal hydraulic jack was load controlled and applied a transverse compressive load to the specimen. The jack was kept in position by means of four steel rods positioned on opposite sides of the specimen, which were in turn kept in position by steel plates (Figure 46). In order to keep the transverse compressive load constant ($\pm 2\%$), a spring system was used between the hydraulic jack and the load cell. The stiffness of the springs was defined on the basis of the required pre-compression level. A load cell was placed between the spring and the steel plate to measure the applied load.

Two vertical LVDTs were attached both on the front and the back side of the specimens, to measure the relative vertical displacement. The horizontal displacement was measured by two horizontal LVDTs on each side. The first three samples were tested using the LVDTs' arrangement shown in Figure 47a. It was observed that apart from crack in the joint, a diagonal crack was formed initiating from the bottom support and normally developed to the middle of the sample. One horizontal LVDT was positioned near to the support in order to record the crack opening (Figure 47b).

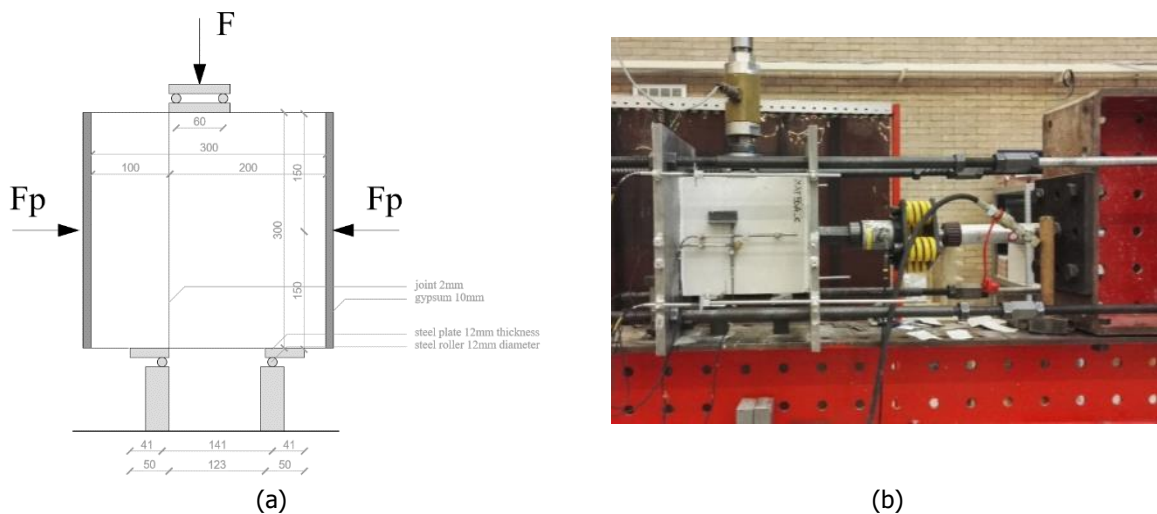


Figure 46 – Shear-compression test on the CS element masonry: (a) adopted specimen; (b) test set-up.



Figure 47 – Arrangement of the LVDT's: (a) measuring system arrangement 1; (b) measuring system arrangement 2.

11.2 Experimental results

During the test, two main cracks occurred (Figure 48 and Figure 49): a first vertical crack at the element-joint interface and a diagonal crack between the bottom and top support in the larger unit of the sample. Occasionally, a horizontal crack occurred in the narrow unit as shown in Figure 49. The shear strength associated with the shear-sliding failure of the mortar-element interface was calculated considering the shear force corresponding to the formation of the vertical crack at the element-joint interface:

$$f_{v,joint} = \frac{F_{joint_crack}}{A_s} \tag{17}$$

where F_{joint_crack} is the first peak load corresponding to the development of the vertical crack in the joint and A_s is the cross sectional area of the specimen parallel to the bed joints.

The pre-compression stress f_p can be calculated for each specimen as follows [16]:

$$f_p = \frac{F_p}{A_s} \tag{18}$$

where F_p is the pre-compression force.

The results of all the tests were plotted in a pre-compressive stress versus shear strength diagram following the Coulomb friction criterion. Considering a linear regression of the data, the initial shear strength f_{v0} and the coefficient of friction μ can be estimated such as the intercept with the vertical axis and the gradient of the line, respectively. The angle of internal friction α was determined as the angle between the regression line and the horizontal axis.

$$f_v = f_{v0} + \mu f_p \tag{19}$$

The residual properties associated to the sliding at the element-joint interface cannot be determined due to the formation of a diagonal crack in the wide unit.



Figure 48 – Typical observed cracks including vertical crack in the joint and diagonal crack in the unit (specimen TUD_MAT-56A-f): (a) front side; (b) back side.

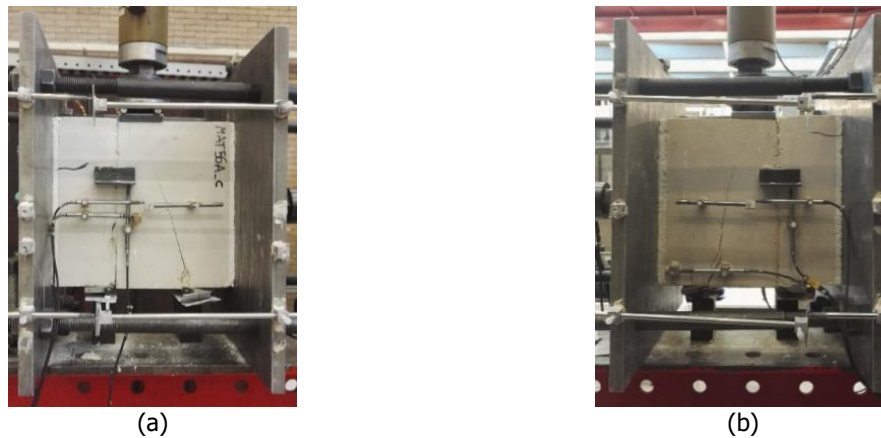


Figure 49 – Developing horizontal crack in the unit (specimen TUD_MAT-56A-c): (a) front side; (b) back side.

Figure 50 shows the shear stress versus relative vertical displacement for the tested specimens by making subdivisions for the three level of pre-compression. Additionally, the observed crack types formation of the vertical diagonal and horizontal cracks are indicated. It is possible to note that the vertical crack at the element-mortar interface occurs in correspondence of a first peak in force. Subsequently, the maximum shear force is reached when the diagonal crack in the wide unit occurs. As explained in the previous paragraph, the first peak corresponding to the formation of the vertical crack is considered for the estimation of the shear properties at element-mortar interface; the residual properties for this interface cannot be estimated due to the mixed failure mode (sliding at the joint and shear failure of the unit).

Table 14 and Figure 51 show the results for the tested specimens. The calcium silicate element masonry showed initial shear strength equal to 0.83 MPa and a coefficient of friction equal to 1.48. These parameters are representative of a shear-sliding failure at the element-mortar interface.

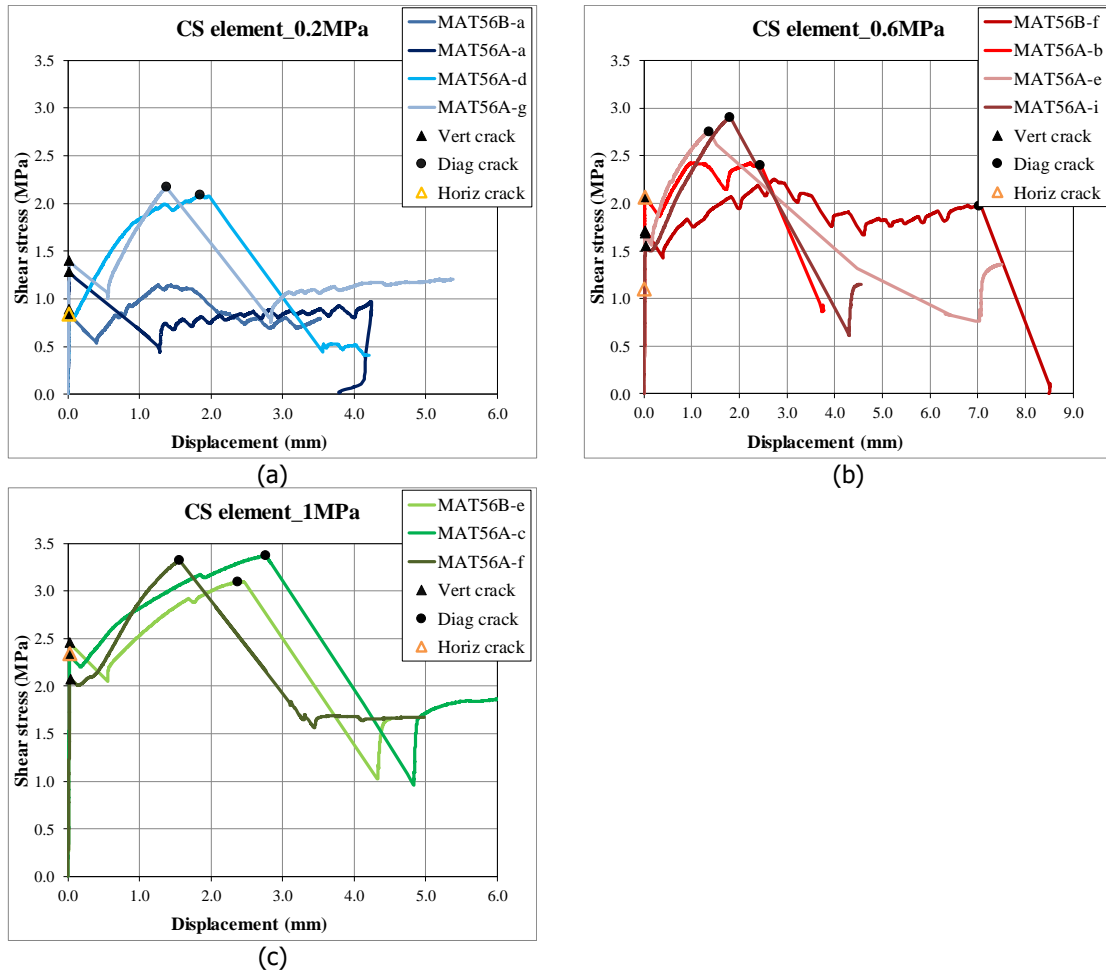


Figure 50 – Shear stress versus relative displacement results: (a) level of pre-compression 0.2MPa; (b) level of pre-compression 0.6MPa; (d) level of pre-compression 1.0 MPa.

Table 14 - Shear strength of calcium silicate element masonry specimens.

$f_p = 0.2 \text{ MPa}$			$f_p = 0.6 \text{ MPa}$			$f_p = 1.0 \text{ MPa}$		
Specimen name	$f_{v,joint}$	$f_{v,diag}$	Specimen name	$f_{v,joint}$	$f_{v,diag}$	Specimen name	$f_{v,joint}$	$f_{v,diag}$
	MPa	MPa		MPa	MPa		MPa	MPa
TUD-MAT-56B-a*	0.84	-	TUD-MAT-56B-f*	1.72	-	TUD-MAT-56B-e	2.45	13.3
TUD-MAT-56A-a*	1.28	-	TUD-MAT-56A-b	2.07	10.3	TUD-MAT-56A-c	2.33	14.4
TUD-MAT-56A-d	0.89	8.9	TUD-MAT-56A-e	1.69	11.8	TUD-MAT-56A-f	2.07	14.2
TUD-MAT-56A-g	1.40	9.3	TUD-MAT-56A-i	1.55	12.5			
Average	1.10	9.1	Average	1.76	11.5	Average	2.29	14.0
St. dev.	0.28	0.25	St. dev.	0.22	1.10	St. dev.	0.19	0.62
C.o.V.	0.25	0.03	C.o.V.	0.13	0.10	C.o.V.	0.09	0.04

* No diagonal crack on the sample

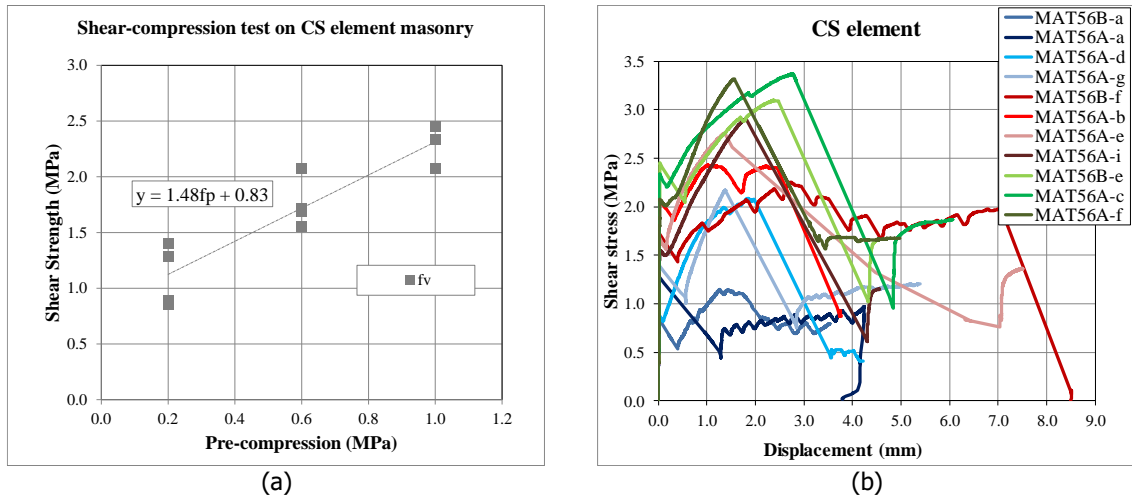


Figure 51 – Shear test results: (a) shear strength versus pre-compression stress; (b) shear stress versus relative displacement (LVDTs' readings).

Table 15 - Shear properties of calcium silicate element masonry.

Property	Symbol	Unit	Calcium silicate masonry
Initial shear strength	f_{v0}	MPa	0.83
Coefficient of friction	μ		1.48
Angle of internal friction	α		56°

12 Comparison with values proposed by standards

Eurocode 6 [2], National Annex to the Eurocode 6 [17], NPR 9096-1-1:2012 [18] and Section 9 in NPR 9998:2017 [19] propose characteristics value of masonry properties to be used in the design procedure. Additionally, the mean values of properties for the existing masonry including subdivision for masonry types and year of the construction are proposed in Appendix F (Table F.2) in NPR 9998:2017 [19]. In this section a comparison between experimental findings and the values proposed by these standards is presented.

12.1 Characteristic compressive strength of masonry

The characteristic compressive strength of masonry can be calculated by following Eurocode 6 and the national annex (Paragraph 3.6.1.2 in [2] or [17]):

$$f_{k,EC6} = K f_b^\alpha f_m^\beta \quad (20)$$

where f_b is the normalised mean compressive strength of the masonry unit, f_m is the compressive strength of mortar, and K , α , β are constants (Table NB-2 in [17]). The normalised mean compressive strength of the masonry unit f_b is determined by multiplying the measured value for the shape factor δ (Table B.1 in [2] or Table NB-A.1 in [17]).

Characteristic strength values of the compressive strength of masonry are also tabulated by the NPR 9096-1-1:2012 [18]. NPR 9998:2017 [19] prescribes minimum characteristics value on the basis of masonry type.

From the experiments, the characteristic compressive strength of masonry is calculated as [10]:

$$f_k = f_m' - 1.645\sigma \quad (21)$$

where f_m' is the mean measured compressive strength and σ is the standard deviation.

Table 16 lists the characteristics compressive strength value of the calcium silicate element masonry. The characteristic compressive strength of masonry has been calculated following the Eurocode 6 and its national annex. The calculations have been carried out both by considering the properties of brick and mortar as declared by the procedure and by using the mean value experimentally determined (Section 4 and 6). Additionally, a comparison with the values prescribes by NPR 9096-1-1:2012 and the minimum values proposed in NPR 9998:2017 (§ 9.3.2.3) is provided.

The experiment provides a higher characteristic value with respect to the prescription of the standards and provides higher value with respect to the minimum values as proposed in NPR 9998:2017.

Table 16 – Characteristic values for the compressive strength of masonry.

				CS element masonry
Compressive strength of mortar	Declared value	f_m	MPa	12.5
	Mean value			16.1
Normalized compressive strength of masonry unit	Declared value	f_b	MPa	12.0
	Mean value			19.4
Characteristic compressive strength of masonry - Eurocode 6		K		0.80
		α		0.85
		β		0
	Declared value	$f_{k,EC6}$	MPa	6.6
	Mean value			9.9
Characteristic compressive strength of masonry - National annex to the Eurocode 6		K		0.80
		α		0.75
		β		0.1
	Declared value	$f_{k,N}$	MPa	6.6
	Mean value			9.8
Characteristic compressive strength of masonry - NPR 9096-1-1:2012		$f_{k,NPR}$	MPa	5.6
Minimum value of the characteristic compressive strength of masonry - NPR 9998:2017 in § 9.3.2.3		$f_{k,NPR9998}$	MPa	6.6
Characteristic compressive strength of masonry - Experiments		f_k	MPa	12.2

12.2 Elastic modulus of masonry

The national annex of Eurocode 6 [17] and the NPR 9998:2017 [19] linearly correlates the elastic modulus of masonry (mean value) to its compressive strength with a constant factor $K_E = 700$.

The elastic modulus of masonry is correlated to the characteristic compressive strength, calculated with Eq. (21), in Table 17. The ratio between stiffness and characteristic strength is approximatively equal to 700.

Table 17 – Ratio between elastic modulus and the characteristic compressive strength of masonry.

Calcium silicate element masonry	Eurocode 6, national annex and NPR 9998:2017	Experiments		
		E_1/f_k	E_2/f_k	E_3/f_k
K_E	700	701	759	681

12.3 Stress-strain relationship for masonry in compression

NPR 9998:2017 [19] proposes the following parabolic curve for the description of the stress-strain relationship in the pre-peak phase:

$$\sigma(\varepsilon) = \left[1 - \left(1 - \frac{\varepsilon}{0.0035} \right)^2 \right] \times f'_m \quad (22)$$

where σ is the compressive stress of masonry and ε is the corresponding strain. According to this expression the strain corresponding to compressive strength is 0.0035. Experimentally an average peak strain value for the calcium silicate element masonry equal to 0.0020 is found (Section 8). The standard overestimates the peak strain of 75% with respect to the experimental findings.

12.4 Characteristic out-of-plane flexural strengths of masonry

Eurocode 6 [2] reports characteristic value for the out-of-plane flexural strengths, while NPR 9096-1-1:2012 [18] and NPR 9998:2017 (§ 9.3.2.3 in [19]) prescribe minimum characteristic values on the basis of the exposure zone and masonry types, respectively. From experiments, the characteristic value is determined by dividing the mean value by the factor 1.5, as prescribed by the testing standard [13].

Table 18 lists the characteristic values for the out-of-plane flexural strengths. Eurocode 6 suggested values of the characteristic flexural strength which are lower than the values found from the experiments. The values proposed in NPR 9096-1-1:2012 and NPR 9998:2017 as minimum values for the characteristic strength are higher than those reported in the experiments.

The orthotropic flexural strength ratio in Eurocode 6 is prescribed as 1.5. This ratio prescribed as 2.0 both in NPR 9096-1-1:2012 and NPR 9998:2017. Experimentally, a ratio equal to 1.3 is obtained.

Table 18 - Characteristic values for the flexural strength of masonry.

				CS element
Flexural strength with the moment vector parallel to the bed joint and in the plane of the wall	Characteristic value by EC6	$f_{x1k,EC6}$	MPa	0.20
	Minimum characteristic value by NPR 9096-1-1:2012	$f_{x1,kNPR}$	MPa	0.60
	Minimum characteristic value by NPR 9998:2017 in	$f_{x1,kNPR9998}$	MPa	0.60
	Experiments	f_{x1k}	MPa	0.39
Flexural strength with the moment vector orthogonal to the bed joint and in the plane of the wall	Characteristic value by EC6	$f_{x2k,EC6}$	MPa	0.30
	Minimum characteristic value by NPR 9096-1-1:2012	$f_{x2k,NPR}$	MPa	1.22
	Minimum characteristic value by NPR 9998:2017	$f_{x2k,NPR9998}$	MPa	1.20
	Experiments	f_{x2k}	MPa	0.49
Ratio f_{x2k} / f_{x1k}	EC6			1.5
	NPR 9096-1-1:2012			2.0
	NPR 9998:2017 in § 9.3.2.3			2.0
	Experiments			1.3

12.5 Characteristic shear properties of masonry

Eurocode 6 [2] and NPR 9096-1-1:2012 report characteristics value only for the initial shear strength, while NPR 9998:2017 (§ 9.3.2.3 in [19]) prescribes minimum characteristics values both for the initial shear strength and coefficient of friction.

From experiments, the characteristic value of the initial shear strength and coefficient of friction is determined as the 80% of the mean measured value, as prescribed by the testing standard [16]. The characteristic initial shear strength values obtained from experiments is approximately 66% higher than the prescribed value by Eurocode 6 and it is 10% higher than the minimum values proposed in NPR 9096-1-1:2012 and NPR 9998:2017 (Table 19). The characteristic coefficient of friction is approximately 50% higher than the minimum value prescribed by NPR 9998:2017 in § 9.3.2.3.

Table 19 - Characteristic shear properties of CS element masonry.

Calcium silicate element masonry	Characteristic initial shear strength	Characteristic coefficient of friction
	MPa	-
	$f_{v0,k}$	μ_k
Characteristic value by EC6	0.40	-
Minimum characteristic value by NPR 9096-1-1:2012	0.60	-
Minimum characteristic value by NPR 9998:2017	0.60	0.78
Experiments	0.66	1.18

12.6 Comparison with Table F.2 in NPR 9998:2017

The mean value of properties for the existing masonry including subdivision for masonry types and year of construction are proposed in Table F.2 (Appendix F) in NPR 9998:2017 [19]. This table was derived based on the test results obtained during the testing campaigns performed in 2014 and 2015 ([20]-[21]), from literature information, scientific judgment and some preliminary results of 2016 testing campaign on the replicated masonry (that were available until April 2017). It is worth noting that for the masonry made of calcium silicate element with thin layer mortar joint, limited information is available for the Dutch existing masonry.

Table 20 lists the mean values from the experiments and the mean values proposed in Table F.2 for the calcium silicate element masonry constructed after 1985. The value reported in Table F.2 NPR 9998:2017 are in line with the experimental data, with the exception of the flexural strength f_{x2} and the fracture energy in parallel to the bed joint for which the standard provides an overestimation.

Table 20 – Comparison between the masonry properties obtained from experiments and the mean values proposed in Table F.2 NPR 9998:2017.

Masonry properties		Symbol	Unit	NPR 9988:2017 Table F.2	Experiment
Compressive strength of masonry	vertical	f_m	MPa	10.0	13.9
	horizontal	$f_{m,h}$			9.42
Elastic modulus of masonry	vertical	E_1	MPa	7500	8557
		E_2			9256
		E_3			8313
	horizontal	$E_{1,h}$	MPa		8416
		$E_{2,h}$			10524
		$E_{3,h}$			7701
Flexural strength with the moment vector parallel to the bed joint and in the plane of the wall		f_{x1}	MPa	0.6	0.58
Flexural strength with the moment vector orthogonal to the bed joint and in the plane of the wall		f_{x2}	MPa	1.0	0.73
Initial shear strength		f_{v0}	MPa	0.8	0.83
Masonry (bed joint) shear friction coefficient		μ	-	0.8	1.48
Fracture energy in bending parallel to the bed joint		G_{fx1}	N/m	20	8.2
Fracture energy in bending perpendicular to the bed joint		G_{fx2}	N/m	20	43.3
Fracture energy in compression	vertical	G_{f-c}	N/m	20000	20900
	horizontal	$G_{f-c,h}$			12800

13 Summary and properties overview

This report concerns with characterisation of the calcium silicate element masonry at material level. This material is frequently applied in the construction of the modern terraced house (after mid-1980) characterised by cavity walls composed of an inner leaf in calcium silicate element masonry and an outer leaf in clay masonry. The knowledge regarding the behaviour of calcium silicate element masonry at material level is limited in the literature. As a result, a complete characterisation of calcium silicate element was performed at material level. In spite of all the difficulties caused during the construction, handling and testing, conforming specimens were adopted in the current study. The material tests were performed within the WP1 of the large-scale testing campaign of 2016 at TU Delft. A characterisation at component level (in-plane and out-of-plane tests) and at assemblage level was also performed in WP3 and WP5 of the same testing campaign, respectively.

Adopting well-designed displacement-control testing set-ups is the privilege of the current study. The compression, bending and shear properties of masonry specimens were measured. The compression tests were performed in two orthogonal directions, perpendicular and parallel to the bed joints, aiming to investigate the orthotropic behaviour of masonry. Both cyclic and monotonic compression tests were performed. The bending properties of the masonry were studied by performing four-point bending tests, both out-of-plane and in-plane, and bond wrench tests. Using the improved testing set-up, horizontal out-of-plane bending tests, where the plane of failure was perpendicular to the bed joints, and vertical out-of-plane bending tests, where the plane of failure was parallel to the bed joints, were performed. In-plane bending test was adopted where the moment vector was orthogonal to the plane of the specimen. In both in-plane and out-of-plane bending tests, the crack opening was used as a controlling parameter allowing an estimation of the post-peak behaviour. The shear properties of masonry were obtained by performing shear tests on couplets. The initial shear parameters, including initial shear strength and coefficient of friction were studied within the framework of the Coulomb friction criterion. Table 21 gives an overview of the obtained properties.

Table 21 – Overview of mechanical properties for calcium silicate element masonry.

Property	Symbol	Unit	Calcium silicate element			
			Average	St. dev.	C.o.V.	No. test
Compressive strength of mortar	f_m	MPa	16.1	1.48	0.09	36
Flexural strength of mortar	f_{mt}	MPa	4.7	1.04	0.22	18
Normalised compressive strength of masonry unit	f_b	MPa	19.4	2.69	0.14	25
Flexural strength of masonry unit	f_{bt}	MPa	3.65	0.21	0.06	18
Elastic modulus of masonry unit in compression	E_b	MPa	8916	7624	0.11	6
Density of masonry	ρ	Kg/m ³	1824	38	0.02	22
Compressive strength of masonry in the direction perpendicular to bed joints	f'_m	MPa	13.93	1.03	0.07	6
Elastic modulus of masonry in the direction perpendicular to bed joints	E_1	MPa	8557	1619	0.19	
	E_2	MPa	9256	2660	0.29	
	E_3	MPa	8313	1251	0.15	
Fracture energy in compression for loading perpendicular to bed joints	G_{f-c}	N/mm	20.9	5.47	0.26	
Poisson ratio of masonry in the direction perpendicular to bed joints	ν		0.21	0.40	0.20	
Strain corresponding to peak strength in compression in the direction perpendicular to bed joints	ϵ_p	‰	2.01	0.37	0.19	
Compressive strength of masonry in the direction parallel to bed joints	$f'_{m,h}$	MPa	9.42	1.63	0.17	6
Elastic modulus of masonry in the direction parallel to bed joints	$E_{1,h}$	MPa	8416	1445	0.17	
	$E_{2,h}$	MPa	10524	1625	0.15	
	$E_{3,h}$	MPa	7701	1502	0.19	
Fracture energy in compression for loading parallel to bed joints	$G_{f-c,h}$	N/mm	12.8	4.34	0.34	
Strain corresponding to peak strength in compression in the direction parallel to bed joints	$\epsilon_{p,h}$	‰	1.58	0.39	0.24	
Masonry flexural strength with the moment vector parallel to the bed joints and in the plane of the wall	f_{x1}	MPa	0.58	0.08	0.14	5
Young's modulus in bending with the moment vector parallel to the bed joints and in the plane of the wall	E_{fx1}	MPa	17620	2400	0.14	
Fracture energy in bending with the moment vector parallel to the bed joints and in the plane of the wall	G_{fx1}	N/mm	0.0082	0.0020	0.24	
Masonry flexural strength with the moment vector orthogonal to the bed joint and in the plane of the wall	f_{x2}	MPa	0.73	0.03	0.04	4
Young's modulus in bending with the moment vector orthogonal to the bed joint and in the plane of the wall	E_{fx2}	MPa	11614	1549	0.13	
Fracture energy in bending with the moment vector orthogonal to the bed joint and in the plane of the wall	G_{fx2}	N/mm	0.0433	0.0112	0.26	
Masonry flexural strength with the moment vector orthogonal to the plane of the wall	f_{x3}	MPa	0.41	0.07	0.17	5
Young's modulus in bending with the moment vector orthogonal to the plane of the wall	E_{fx3}	MPa	7048	1970	0.28	
Flexural bond strength	f_w	MPa	0.55	0.09	0.17	20
Masonry (bed joint) initial shear strength	f_{v0}	MPa	0.83	-	-	11
Masonry (bed joint) shear friction coefficient	μ		1.48	-	-	

Eventually, the experimental results have been compared in terms of characteristic value with the analytical formulation available in standards, such as Eurocode 6 [2], Dutch national annex to Eurocode 6 [17], NPR 9096-1-1:2012 [18] and NPR 9998:2017 (section 9.3.2.3) [19]. A comparison in terms of mean values has been carried out considering Annex F of NPR 9998:2017 [19].

A comparison between the results of the experiments and the values proposed in the standards, both for the characteristic and mean values is shown in Table 22.

The experiments show higher values of the characteristic compression strength with respect to the standards, while a good agreement is found with respect to the ratio between the Young's modulus and the characteristic compressive strength. An overestimation of the strain corresponding to the compressive strength is reported.

Concerning the ratio between the characteristic horizontal bending strength and the characteristic vertical bending strength, an acceptable correspondence between experimental results and the values proposed by Eurocode 6 is found. While, NPR 9096-1-1:2012 and NPR 9998:2017 which prescribe minimum strength values give an overestimation of the properties.

The characteristic initial shear strength and the characteristic coefficient of friction obtained from the experiments are higher than the values suggested in the Eurocode 6 and the minimum values proposed in NPR 9096-1-1:2012 and NPR 9998:2017.

Considering the mean value of the properties as reported in Annex F of NPR 9998:2017, a good agreement can be found, with the exception of the flexural strength f_{x2} and the fracture energy in parallel to the bed joint for which the standard provides an overestimation. It should be pointed out that the mean values reported in Annex F are partially derived from the experimental results presented in this report.

Table 22 – Comparison between the masonry properties obtained from experiments and the characteristic and mean values proposed in the standards.

Masonry properties	Characteristic value						Mean value		
	Symbol	Eurocode 6	Dutch national annex	NPR 9096-1-1:2012	NPR 9998:2017 (§ 9.3.2.3)	Experiment	Symbol	NPR 9998:2017 Table F.2 in Appendix F	Experiment
Compressive strength of masonry(MPa)	f_k	9.9	9.8	5.6	6.6	12.2	f_m	10.0	13.9
Chord elastic modulus of masonry (MPa)	-	-	-	-	-	-	E_3	7500	8313
Ratio between Young's modulus and characteristic/mean compressive strength	E_1/f_k	700	-	700	700	701	E_1/f_m	750	614
	E_2/f_k	700	-	700	700	759	E_2/f_m		664
	E_3/f_k	700	-	700	700	681	E_3/f_m		597
Flexural strength with the moment vector parallel to the bed joint and in the plane of the wall (MPa)	$f_{x1,k}$	0.2	-	0.6	0.6	0.39	f_{x1}	0.60	0.58
Flexural strength with the moment vector orthogonal to the bed joint and in the plane of the wall (MPa)	$f_{x2,k}$	0.3	-	1.2	1.2	0.49	f_{x2}	1.0	0.73
Ratio between horizontal out-of-plane bending and vertical out-of-plane bending	$f_{x1,k}/f_{x2,k}$	1.5	-	2.0	2.0	1.3	f_{x1}/f_{x2}	1.67	1.3
Initial shear strength (MPa)	$f_{v0,k}$	0.40	-	0.6	0.6	0.66	f_{v0}	0.80	0.83
Coefficient of friction	μ_k	-	-	-	0.78	1.18	μ	0.80	1.48
Fracture energy in bending parallel to the bed joint (N/m)							G_{fx1}	20	8.2
Fracture energy in bending perpendicular to the bed joint(N/m)							G_{fx2}	20	43.3
Fracture energy in compression (N/m)	loading direction perpendicular to the bed joint						$G_{f\epsilon}$	20000	20900
	loading direction parallel to the bed joint						$G_{f\epsilon,h}$		12800

References

- [1] Ham, P. Esposito, R. (2016). Material characterisation of replicated calcium silicate element masonry. Delft University of Technology. Report number C31B67WP5-2, version 1, 18 August 2016.
- [2] EN 1996-1-1+A1 (2013). Eurocode 6 – Design of masonry structures – Part 1-1: General rules for reinforced and unreinforced masonry structures. Nederlands Normalisatie-instituut (NEN).
- [3] Protocol for the construction of masonry, ver. 18-03-2015.
- [4] EN 1015-3 (1999). Method of test for mortar for masonry – Part 3: Determination of consistence of fresh mortar (by flow table). Nederlands Normalisatie-instituut (NEN).
- [5] EN 1015-11 (1999). Method of test for mortar for masonry – Part 11: Determination of flexural strength of hardened mortar. Nederlands Normalisatie-instituut (NEN).
- [6] NEN 6790 (2005). Technical principles for building structures - TGB 1990 - Masonry structures - Basic requirements and calculation methods. Nederlands Normalisatie-instituut (NEN).
- [7] EN 772-1 (2000). Methods of test for masonry units - Part 1: Determination of compressive strength. Nederlands Normalisatie-instituut (NEN).
- [8] EN 771-2 (2011). Specification for masonry units - Part 2: Calcium silicate masonry units. Nederlands Normalisatie-instituut (NEN).
- [9] Ad Vermeltfoort. (2005). Brick-mortar interaction in masonry under compression, PhD thesis, Eindhoven University of Technology.
- [10] EN 1052-1 (1998). Method of test masonry – Part 1: Determination of compressive strength. Nederlands Normalisatie-instituut (NEN).
- [11] Van Mier, J.G.M. (1984). Strain Softening of concrete under multiaxial loading conditions, PhD thesis, Eindhoven University of Technology.
- [12] Lourenco, P.B., De Borst, R. and Rots, J.G. (1997). A plane stress softening plasticity model for orthotropic materials. International Journal for Numerical Methods in Engineering 40(21), 4033-4057.
- [13] EN 1052-2 (1999). Method of test masonry – Part 2: Determination of flexural strength. Nederlands Normalisatie-instituut (NEN).
- [14] Pluijm R. Out-of-plane bending of masonry behaviour and strength: Technische Universiteit Eindhoven; 1999.
- [15] EN 1052-5 (2005). Method of test masonry – Part 5: Determination of bond strength by bond wrench method. Nederlands Normalisatie-instituut (NEN).
- [16] EN 1052-3 (2002). Method of test masonry – Part 3: Determination of initial shear strength. Nederlands Normalisatie-instituut (NEN).
- [17] NEN-EN 1996-1-1+C1/NB (2011). National Annex to NEN-EN 1996-1-1+C1 Eurocode 6: Design of masonry structures – Part 1-1: General rules for reinforced and unreinforced masonry structures. Nederlands Normalisatie-instituut (NEN) (in Dutch).
- [18] NPR 9096-1-1 (2012). Masonry structures – Simple design rules, based on EN 1996-1-1+C1. Nederlands Normalisatie-instituut (NEN) (in Dutch).
- [19] NPR 9998:2017. Assessment of buildings in case of erection, reconstruction and disapproval – Basic rules for seismic actions: induced earthquakes (NEN) (in Dutch).
- [20] Jafari S. J.G. Rots and L. Panoutsopoulou. Tests for the characterisation of original Groningen masonry. Delft University of Technology. Dept. Structural Engineering. 18 December 2015.
- [21] Jafari S. J.G. Rots. Summary report for the characterization of original Groningen masonry. 18 December 2015.

Appendix A

This appendix reports the declaration of performance for the construction materials used during the experimental campaign.

Table A.1 refers to the calcium silicate element.

Table A.2 lists the characteristic of mortars for calcium silicate element masonry.

Table A.1 – Declaration of performance of calcium silicate element.

PRESTATIEVERKLARING DÉCLARATION DES PERFORMANCES		31200316	Pagina 1/2 Page 1/2
1.	Unieke identificatiecode van het producttype: Code d'identification unique du produit type:	Element CS12	
2.	Type-, partij- of serienummer, dan wel een ander identificatiemiddel voor het bouwproduct, zoals voorgeschreven in artikel 11, lid 4: Numéro de type, de lot ou de série ou tout autre élément permettant l'identification du produit de construction, conformément à l'article 11, paragraphe 4:	NL014054642015164 NL024054642015164 NL064054642015164	
3.	Beoogde gebruiken van het bouwproduct, overeenkomstig de toepasselijke geharmoniseerde technische specificatie, zoals door de fabrikant bepaald:	In wanden, kolommen en scheidingswanden uit metselwerk	
	Usage ou usages prévus du produit de construction, conformément à la spécification technique harmonisée applicable, comme prévu par le fabricant:	Murs, poteaux et cloisons en maçonnerie	
4.	Naam, geregistreerde handelsnaam of geregistreerd handelsmerk en contactadres van de fabrikant, zoals voorgeschreven in artikel 11, lid 5:	Xella Nederland bv Mildijk 141 4214 DR Vuren Nederland	
	Nom, raison sociale ou marque déposée et adresse de contact du fabricant, conformément à l'article 11, paragraphe 5:		
5.	Indien van toepassing, naam en contactadres van de gemachtigde wiens mandaat de in artikel 12, lid 2, vermelde taken bestrijkt:	Xella Technologie- und Forschungsgesellschaft mbH Hohes Steinfeld 1 D-14797 Kloster – Lehnin	
	Le cas échéant, nom et adresse de contact du mandataire dont le mandat couvre les tâches visées à l'article 12, paragraphe 2:		
6.	Het systeem of de systemen voor de beoordeling en verificatie van de prestatiebestendigheid van het bouwproduct, vermeld in bijlage V:	System 2+ op basis van Categorie I in overeenstemming met EN 771-2 (2011)	
	Le ou les systèmes d'évaluation et de vérification de la constance des performances du produit de construction, conformément à l'annexe V:	System 2+ base sur la Catégorie I conformément à EN 771-2 (2011)	
7.	Indien de prestatieverklaring betrekking heeft op een bouwproduct dat onder een geharmoniseerde norm valt:	IKOB-BKB, Ringveste1, 3992DD, Houten, Nederland, Kennr. 0957 heeft onder System 2+ de volgende taken uitgevoerd: initiële keuring van de fabriek en de productiecontrole evenals het doorlopend toezicht, de beoordeling en de goedkeuring van de FPC en heeft het conformiteitscertificaat van de FPC verstrekt.	
	Dans le cas de la déclaration des performances concernant un produit de construction couvert par une norme harmonisée:	IKOB-BKB, Ringveste1, 3992DD, Houten, Nederland, Kennr. 0957 a réalisé selon le Système 2+ les tâches suivantes : l'inspection initiale, de l'usine et du contrôle, le contrôle continu du FPC et a délivré le certificat de conformité du contrôle de la production en usine.	
8.	Verklaarde prestatie Performances déclarées	Element CS12	
	Afmetingen lengte Dimensions longueur	897 mm ± 2 mm	
	Afmetingen breedte Dimensions largeur	120 mm ± 2 mm	
	Afmetingen hoogte Dimensions hauteur	643 mm ± 1 mm	
	Vormkenmerken Forme	Rechthoekig – kan op verzoek worden aangevraagd Rectangulaire - peuvent être obtenues sur demande	
	Toleranties (lengte / breedte / hoogte) Tolérances ((longueur x largeur x hauteur)	± 2 mm, ± 2 mm, ± 1 mm	EN 771-2, Tabel 1

8.	Kategorie Categorie	T 2	EN 771-2, Tabel 1
	Gemiddelde druksterkte Résistance à la compression moyenne	15 N/mm ² ⌞ Legvlakken, op prisma ⌞ Face de pose, portion d'éprouvette	EN 772-1
	Gemiddelde genormaliseerde druksterkte Résistance à la compression normalisée	12 N/mm ² ⌞ Legvlakken ⌞ Face de pose	EN 772-1
	Afschuifhechtsterkte Résistance de l'adhérence au cisaillement	0,3 N/mm ²	EN 998-2 Bijlage C art.5.4.2.b.
	Bruto (schijnbare) droge volumemassa Masse volumique sèche brute (apparente)	1658 tot/à 1875 kg/m ³	EN 772-13
	Gedrag bij brand Réaction au feu	Euro klasse A1 Euro classe A1	EN 13501-1
	Waterdampdoorlatendheid Perméabilité à la vapeur d'eau	5/25	EN 1745 Tab A.2
	Warmtegeleidingscoëfficiënt Coefficient de conductivité thermique		
	λ_{10dry} (P=90%)	0,75 W/mK	EN 1745 Tab A.2
	λ_{10dry} (P=50%)	0,7 W/mK	EN 1745 Tab A.2
	Duurzaamheid (vorst-dooi weerstand) Durabilité (résistance gel-dégel)	NPD	EN 772-18
	Gevaarlijke stoffen Substances dangereuses	Veiligheidsinformatieblad op aanvraag Fiche de données de sécurité sur demande	

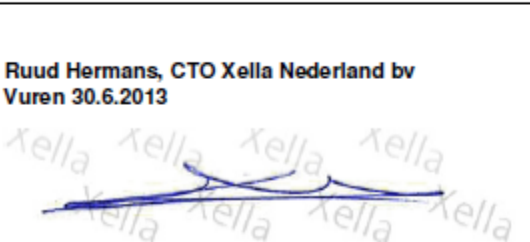
9.	Aanvullende informatie van de producent Informations complémentaires auprès du fabricant	
	Praktische volumieke massa (geluidisolatie) Pratique densité (isolation acoustique)	1750 kg/m ³

10.	De prestaties van het in de punten 1 en 2 omschreven product zijn conform de in punt 9 aangegeven prestaties. Deze prestatieverklaring wordt verstrekt onder de exclusieve verantwoordelijkheid van de in punt 4 vermelde fabrikant. Ondertekend voor en namens de fabrikant door:	Ruud Hermans, CTO Xella Nederland bv Vuren, 30.6.2013
	Les performances du produit identifié aux points 1 et 2 sont conformes aux performances déclarées indiquées au point 9. La présente déclaration des performances est établie sous la seule responsabilité du fabricant identifié au point 4. Signé par le fabricant et en son nom par:	

Table A.2 – Declaration of performance for calcium silicate element masonry mortar.



Prestatieverklaring DECLARATION OF PERFORMANCE		31900017	Bladzijde 1/2 Page 1/2
1.	Unieke identificatiecode van het producttype: <i>Unique identification code of the product-type:</i>	Silkafix zomermortel	
2.	Type-, partij- of serienummer, dan wel een ander identificatiemiddel voor het bouwproduct, zoals voorgeschreven in artikel 11, lid 4: <i>Type-, batch- or serial number or other marking for the identification of the construction product in accordance with Article 11 paragraph 4:</i>	NL004054649004659	
3.	Beoogde gebruiken van het bouwproduct, overeenkomstig de toepasselijke geharmoniseerde technische specificatie, zoals door de fabrikant bepaald: <i>Intended use or uses defined by the manufacturer of the construction product in accordance with the applicable technical specification:</i>	Fabrieksmatig geproduceerde ljm-mortel met vastgelegde eigenschappen voor het verlijmen van metselwerk wanden, kolommen en scheidingsen met kalkzandsteen metselwerk producten overeenkomstig EN 998-2 <i>Factory made designed thin-layer masonry mortar for bedding for use in masonry walls, columns and partitions of calcium-silicate masonry units according EN 998-2</i>	
4.	Naam, geregistreerde handelsnaam of geregistreerd handelsmerk en contactadres van de fabrikant, zoals voorgeschreven in artikel 11, lid 5: <i>Name, registered trade name or trade mark and contact address of the manufacturer in accordance with Article 11, paragraph 5:</i>	Xella Nederland bv Mildijk 141 4214 DR, Vuren Nederland	
5.	Naam en contactadres van de gemachtigde wiens mandaat de in artikel 12, lid 2, vermelde taken bestrijkt: <i>Name and contact address of the authorised representative, who is in charge for the tasks referred to in Article 12, paragraph 2:</i>	Xella Technologie- und Forschungsgesellschaft mbH Hohes Steinfeld 1 D-14797 Kloster – Lehnin Duitsland	
6.	Het systeem of de systemen voor de beoordeling en verificatie van de prestatiebestendigheid van het bouwproduct, vermeld in bijlage V: <i>System or systems of assessment and verification of constancy of performance of the construction product in accordance with Annex V</i>	Systeem 2+ op basis van een mortel met vastgestelde eigenschappen in overeenstemming met EN 998-2 (2010) <i>System 2+ on the basis of designed mortar in accordance with EN 998-2 (2010)</i>	
7.	Indien de prestatieverklaring betrekking heeft op een bouwproduct dat onder een geharmoniseerde norm valt: <i>In case of the declaration of performance concerns a construction product covered by a harmonised standard</i>	IKOB-BKB, Ringveste 1, 3992 DD, Houten, Nederland, met code NB0957, heeft onder System 2+ de volgende taken uitgevoerd: initiele keuring van de fabriek en de fabriekseigen productiecontrole (FPC), het doorlopend toezicht, de beoordeling en de goedkeuring van de FPC en heeft het conformiteitscertificaat van de FPC verstrekt. <i>IKOB-BKB, Ringveste 1, 3992 DD, Houten, Nederland, with code NB0957 has performed, based on system 2+, the following tasks: the initial inspection of the factory and the factory production control (FPC), continuously surveillance, assessment and approval of F.P.C. and issued the F.P.C. certificate.</i>	
8.	Verklaarde prestatie <i>Declared performance</i>	Silkafix zomermortel	
	Druksterkte <i>Compressive strength</i>	≥ 12,5 N/mm²	EN 1015-11
	Hechtsterkte (afschuifsterkte) <i>Bond strength (initial shear strength)</i>	≥ 0,3 N/mm²	Tabulated value EN998-2, Annex C
	Chloride gehalte <i>Contents of chlorides</i>	< 0,1 %_m	EN 1015-17
	Gedrag bij brand <i>Reaction to fire</i>	A1	EN 13501-1
	Waterabsorptie <i>Water absorption</i>	Geen prestatie bepaald (GPB / NPD)	EN 1015-18
	Waterdampdoorlatendheid <i>Water vapour permeability</i>	5 / 20	Tabulated value EN 1745, Table A.12
	Warmtegeleidingscoëfficiënt <i>Thermal conductivity/Density</i>	λ_{10dry} (p=50%) : 0,49 W/mK λ_{10dry} (p=90%) : 0,53 W/mK	Tabulated value EN 1745, Table A.12

Prestatieverklaring DECLARATION OF PERFORMANCE		Silkafix zomermortel	Bladzijde 2/2 Page 2/2
8.	Duurzaamheid <i>Durability</i>	De praktijk toont aan, dat bij gebruik overeenkomstig de bedoelde toepassing de mortel een hoge vorst/dooi-bestandheid heeft. <i>History has shown, that the mortar has a high freeze-thaw resistance when applied in the intended place of use.</i>	
	Gevaarlijke stoffen <i>Dangerous substances</i>	Veiligheidsblad op aanvraag <i>Safety data sheet on request</i>	
9.	Aanvullende informatie van de producent <i>Additional information given by the manufacturer</i>	Het materiaal moet tijdens transport en opslag worden beschermd tegen vocht en vorst <i>The material has to be protected against moisture and frost during transport and storage.</i>	
	Hechtsterkte (kruisproef) <i>Bond strength</i>	≥ 0,40 N/mm ²	
	Verwerkingstijd in uren <i>Workable life in hours</i>	≥ 4	EN 1015-9
	Open tijd in minuten <i>Correction time in minutes</i>	≥ 7	EN 1015-9
	Droge volumieke massa <i>Dry bulk density</i>	1.450 +/- 50 kg/m ³	EN 1015-10
10.	De prestaties van het in de punten 1 en 2 omschreven product zijn conform de in punt 8 aangegeven prestaties Deze prestatieverklaring wordt verstrekt onder de exclusieve verantwoordelijkheid van de in punt 4 vermelde fabrikant:	<p>Ruud Hermans, CTO Xella Nederland bv Vuren 30.6.2013</p> 	
	<i>The performance of the product referring to paragraph 1 and 2 correspond to the declared performance at paragraph 8. This declaration of performance was issued under the sole responsibility of the manufacturer specified in paragraph 4. Signed on behalf of the manufacturer</i>		